PAPER Special Section on Wide Band Systems

Characteristics of Dual Frequency Planar Monopole Antenna for UWB System

Yuko RIKUTA[†a)], *Member and* Ryuji KOHNO[†], *Fellow*

SUMMARY An antenna with a wide bandwidth is required for ultra-wideband (UWB) system of the future. Several types of wideband antenna that cover the whole frequency range have been proposed. Since the UWB system would cover from 3.1 to 10.6 GHz, it is necessary to suppress the interference from other systems using some of this frequency band. This paper presents two types of novel planar monopole antenna: one consists of two connected rectangular plates and another one is an orthogonal type. The return loss characteristics, radiation pattern, and current distribution of these antennas were simulated by using the FDTD method. The proposed antennas had dual frequency and broad bandwidth characteristics at both resonant frequencies. The return loss level at the eliminated frequency between the resonant frequencies was almost 0 dB. The radiation patterns for the whole frequency range were almost omni-directional in the horizontal plane. The current distributions at each frequency were similar to that of a planar rectangular monopole. The radiation patterns thus were omni-directional in the horizontal plane at each resonant frequency. Therefore, the results showed that wide bandwidth characteristics could be achieved with such antennas.

key words: monopole antenna, dual frequency, omni-directional, ultra-wideband, FDTD method

1. Introduction

Several types of wideband antenna have been proposed for future ultra-wideband (UWB) systems [1]–[5]. These antennas must be able to cover the entire frequency range of the system and can be classified as to their structure; that is, they have either a three-dimensional structure or a planar structure. The three-dimensional antennas include the double-ridged guided horn antenna (DRGHA), the log-periodic antenna, and the monocone-like antenna (tear-drop shaped) [1]. The planar antennas include the Vivaldi antenna, the planar dipole antenna (e.g., bow-tie), the planar monopole antenna, and the fractal antenna [2]–[5]. Not only the standard antennas but also smaller ones for PC cards, Compact Flash, etc., as well as ones for base station antennas have been studies in the above research. The latter antennas were the subjects of the work presented in the current paper.

Since the UWB system would cover the frequency band from 3.1 to 10.6 GHz, it is necessary to suppress interference from other systems using some of this frequency band. For instance, the frequency band of about 5–6 GHz is used for wireless LAN systems. An antenna with a dual frequency capability and a wide bandwidth at both resonant frequencies must be able to suppress parts of the 3.1 to 10.6 GHz frequency band. While it is possible to use two wideband antennas (one for each frequency band), these would take up more space than would one dual frequency antenna.

One way to make a dual frequency antenna is to place a parasitic element near the radiation part. By using parasitic elements, other resonances occur, for which dual or multiple frequency characteristics can be obtained [6].

Another antenna with dual frequency characteristics and a two-layer geometry is described in [7]. This stacked antenna consists of a lower top loaded monopole antenna and an upper element. The upper element is connected to the lower antenna by a short pin at the center of the lower element. The dual frequency characteristic in this case is due that the antenna can be viewed as two top loaded monopole antennas. Moreover, the radiation characteristics at each resonant frequency are omni-directional in the horizontal plane, since each pattern is radiated from each top loaded monopole antenna. However, the bandwidth at each resonant frequency is less than 500 MHz, obviously not broad enough to cover the UWB frequency range. These antennas are thus suitable for two narrowband applications but not for two wideband applications.

To solve the above problems, this paper proposes two types of novel planar rectangular monopole antenna, each with dual frequency, wideband characteristics and an omni-directional radiation pattern in the horizontal plane. The return loss characteristics, radiation patterns, and current distribution of these antennas were calculated by using the finite difference time domain (FDTD) method.

2. Planar Rectangular Monopole Antenna

The planar rectangular monopole antenna was analyzed and compared with a wire monopole. The analysis model of the antenna is shown in Fig. 1. An infinite ground plane was assumed. The height of the rectangular monopole was $H = 22$ mm, the width was W, and the length of the feed pin was $g = 1$ mm. The size of the rectangular part was $(H - g) \times W$. The antenna characteristics were simulated by using the FDTD method. The FDTD parameters are shown in Table 1. An eight-layer PML (perfect matching layer) was used as the absorbing boundary condition (A. B. C.).

Figure 2 shows the return loss characteristics of the planar monopole antenna for different monopole widths

Manuscript received February 23, 2004.
Manuscript revised May 23, 2004.
Final manuscript received June 21, 2004.

[†]The authors are with UWB Technology Institute, National Institute of Information and Communications Technology, Yokosuka-shi, 239-0847 Japan.
a) E-mail: rikuta@nict.go.jp

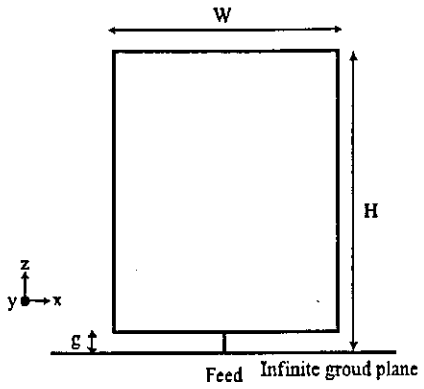

Fig. 1 Geometry of planar rectangular monopole antenna.

Table 1 Analysis parameters.

Cell size	Δx=Δy=1.0 mm Δz=0.5 mm
Iteration	5000
Incident wave	Gaussian pulse
A. B. C.	PML 8 layer

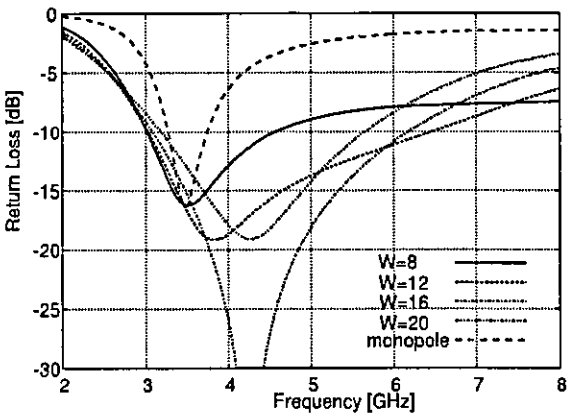

Fig. 2 Return loss characteristics of planar monopole antennas with different widths W.

W. H was fixed at 20 mm for the resonant frequency of about 3.5 GHz. By increasing the width so that the antenna becomes rectangular, the antenna characteristics become wideband and the return loss levels change because of the change in impedance matching. It is evident that the planar monopole has a wider bandwidth than that of a wire monopole. If the return loss is suppressed to less than −10 dB, which is approximately equivalent to VSWR (Voltage Standing Wave Ratio) < 2, the maximum bandwidth is from 3.0 to 6.4 GHz for W = 12 mm.

The radiation characteristics of the planar rectangular monopole antenna when W = 12 mm are shown in Fig. 3. These characteristics are in the horizontal plane at 3.0, 4.0, 5.0, 6.0 GHz. At these frequencies, this antenna model gives a return loss of less than −10 dB. The cross-polarization characteristics of the antenna at each frequency are suppressed to less than −20 dBi (not shown in this figure). The

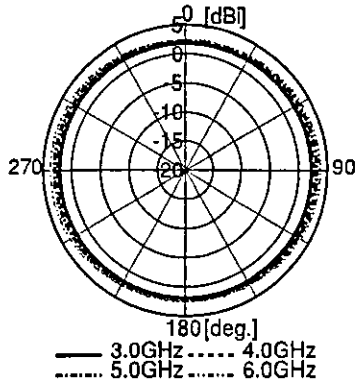

Fig. 3 Radiation characteristics of planar monopole antenna in the horizontal plane (xy-plane).

radiation patterns are similar to that of a monopole antenna, and they become slightly distorted at the higher frequency range.

3. Planar Monopole Antenna

3.1 Antenna Structure

Figure 4 shows the analysis model of the novel dual frequency planar monopole antenna. The antenna consists of an upper and lower part connected by a pin and is formed by making slits in the vertical edges of the planar rectangular monopole antenna shown in Fig. 1. That is, the pin is formed by making the distance between both slits thin like a wire. For the simplicity of analysis, the shape of each antenna element is considered to be rectangular. An infinite ground plane is also assumed. The planar monopole height is denoted as H and the length of feed pin is g = 1 mm. The upper and lower rectangular areas are $H_u \times W_u$ and $H_l \times W_l$, respectively. The length of the pin is z. Thus, $H = H_u + z + H_l + g$. The antenna characteristics were simulated by using FDTD method. The FDTD parameters were the same as shown in Table 1.

3.2 Antenna Characteristics

This section examines the influence of the cut-out slits on the characteristics of the planar rectangular monopole antenna. The heights and widths are fixed as H = 20 mm, W = $W_u = W_l$ = 12 mm, z = 4 mm, H_u = 2 mm, and H_l = 13 mm.

Figure 5 shows the return loss characteristics of the planar monopole with slits (novel) and without slits. As can be seen, the novel planar monopole antenna has dual frequency characteristics. At the lower and higher resonant frequencies, this antenna has broadband characteristics. The return loss level is suppressed to less than −10 dB, from about 3 to 4 and 7.5 to 10 GHz, or from 2.5 to 5 and 7 to 11 GHz for VSWR < 3, while the level between resonant frequencies is increased to over −3 dB, reaching almost 0 dB.

The radiation characteristics of the novel dual frequency planar monopole antenna are shown in Fig. 6. These

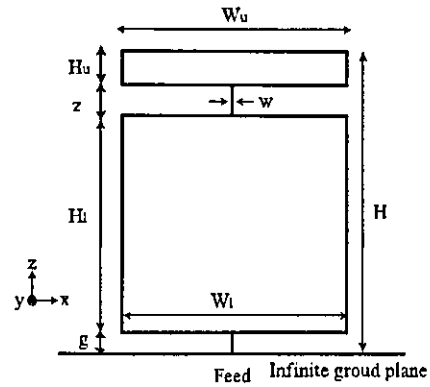

Fig. 4 Geometry of novel dual frequency planar monopole antenna (upper element: rectangle, lower element: rectangle).

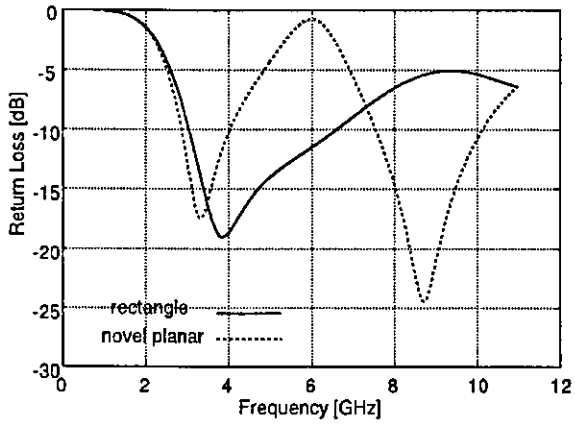

Fig. 5 Return loss characteristics of the antenna structures.

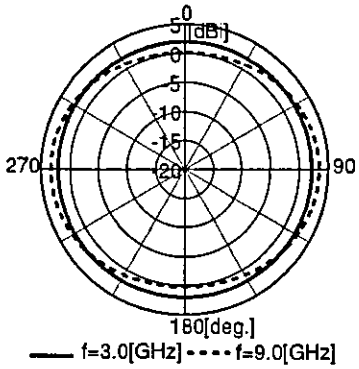

Fig. 6 Radiation characteristics of dual-frequency planar monopole in the horizontal plane (*xy*-plane).

characteristics are in the horizontal plane for frequencies of 3.0 and 9.0 GHz, which are respectively near the lower and upper resonant frequency. The cross polarization characteristics are suppressed to less than −20 dBi (not shown). The radiation patterns at each frequency are similar to that of a monopole antenna, that is, approximately omni-directional in the horizontal plane. There is a small amount of distortion in the radiation pattern of the higher resonant frequency.

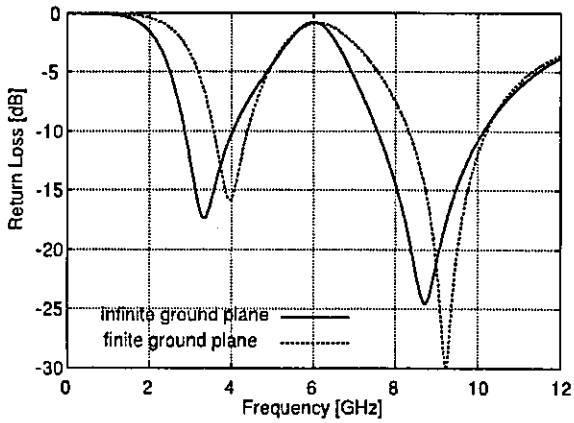

Fig. 7 Return loss characteristics according to type of ground plane.

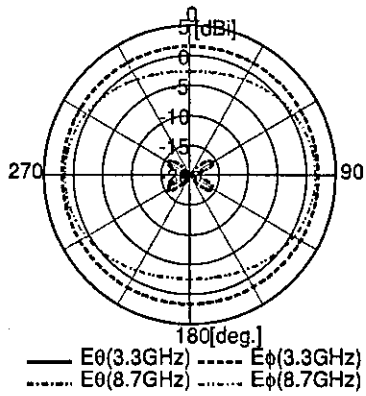

Fig. 8 Radiation characteristics in the horizontal plane (*xy*-plane).

Figure 7 shows the return loss characteristics of the planar monopole antennas shown in Fig. 4 when the ground plane is the finite type or the ideal infinite type. The finite ground plane was 20 mm square. Both planar monopole antennas (i.e., using an infinite or finite ground plane) have dual frequency characteristics with a wide bandwidth. The return loss level between each resonant frequency exceeds −3 dB, reaching almost 0 dB.

Figure 8 shows the radiation characteristics of the planar monopole antenna when the ground plane is finite. These characteristics are in the horizontal plane with frequencies of 3.3 and 8.7 GHz. When using an infinite ground plane, the cross polarization characteristics at each frequency are suppressed to less than −20 dBi. On the other hand, the level of cross polarization when using a finite ground plane is suppressed to less than −20 dBi at the lower frequency and less than −15 dBi at the higher resonant frequency. Even though the cross polarization characteristics do depend somewhat on the ground plane type, for simplicity of analysis, the infinite ground plane can be assumed in the following.

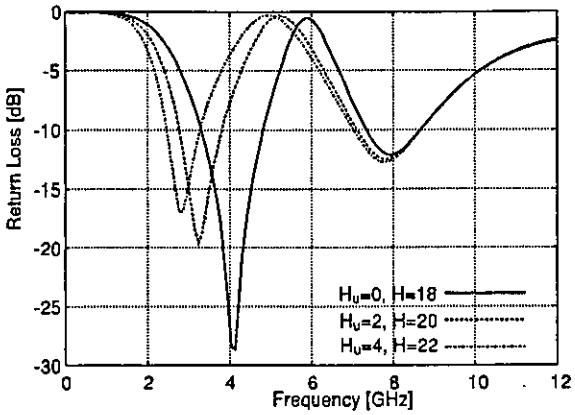

Fig. 9 Return loss characteristics for different upper element heights H_u.

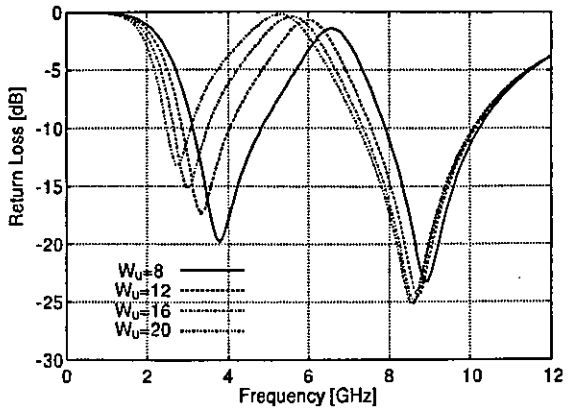

Fig. 10 Return loss characteristics for different upper element widths W_u.

3.3 Return Loss Characteristics

The return loss characteristics are examined according to the antenna parameters of the dual frequency planar monopole antenna. The antenna impedance is affected by changing the feed pin length g. If the detail of the feed part is taken to be a parameter, it is difficult to model the feed part and analyze it by using the FDTD method unless the subcell technique, non-uniform mesh, etc. are used. For the simplicity then, g is fixed at 1 mm.

Figure 9 shows the return loss characteristics for different upper element heights H_u. This antenna's widths are $W_u = W_l = 16$ mm. $z = 4$ mm, and H_l is fixed at 13 mm. H_u is a variable; therefore, when it increases, the antenna's overall height H also increases, while the lower element's height does not change. $H_u = 0$ means that the upper element is a wire. This planar monopole antenna has dual frequency characteristics and wideband characteristics at each resonant frequency. The return loss level at the eliminated frequencies between the resonant ones increases to over −3 dB, reaching almost 0 dB. When H_u goes from 0 mm to 4 mm, i.e., H goes from 18 mm to 22 mm, the lower resonant frequency shifts to a lower value, from around 4 GHz to 3 GHz. The return loss level of the lower frequency also changes because of the change in the impedance matching. On the other hand, the higher resonant frequency is not influenced by changing H_u and H.

Figure 10 shows The return loss characteristics for different upper element widths W_u. W_u is a variable, while $W_l = 12$ mm. $z = 4$ mm, H_l is 13 mm, and H_u is 2 mm. When W_u goes from 8 mm to 20 mm, the lower resonant frequency shifts to a lower value and the bandwidth decreases. On the other hand, the higher resonant frequency is almost unaffected by changing W_u.

The return loss characteristics for different connector pin widths w are shown in Fig. 11. Changing the width of the connector pin is the same as changing the depth of the slits. When the pin becomes as thin as a wire, dual frequency characteristics become evident and the higher resonant frequency appears. On the other hand, the lower resonant frequency is almost unaffected by changing w.

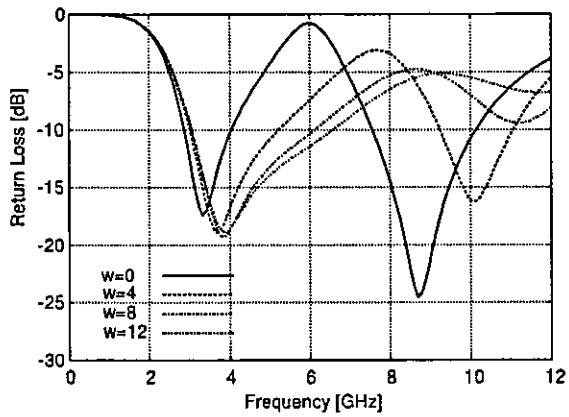

Fig. 11 Return loss characteristics for different connector pin widths w.

Thus by changing each antenna element's height, that is H_u, z, or H_l, the lower resonant frequency is not much influenced if the total antenna height H is fixed. However, the higher resonant frequency does depend on the height of the lower rectangle H_l. Changing the widths of the antenna elements affects the bandwidth characteristics at each frequency, the same as in the planar rectangular monopole antenna case.

3.4 Comparison of Analysis and Measurement Result

Figure 12 shows the dual frequency planar monopole antenna with a wire-like upper element that was used in the measurement. The height and widths were $H = 17$ mm and $W_u = W_l = 16$ mm, and $z = 5$ mm, $H_l = 12$ mm, and H_u was infinitesimal (=0). The lower part was rectangular, as in Fig. 4. The ground plane was finite in the measurement.

Figure 13 shows the simulated and measured return loss characteristics of the experimental antenna. The antenna had dual frequency characteristics and wideband characteristics at the lower and higher resonant frequency. The

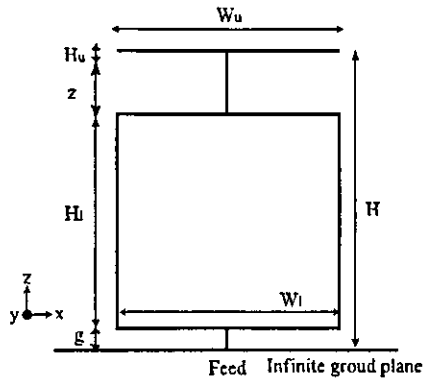

Fig. 12 Geometry of experimental dual frequency planar monopole antenna (upper element: wire, lower element: rectangle).

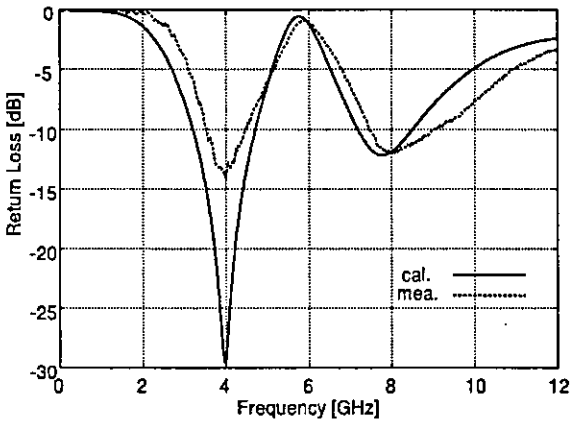

Fig. 13 Return loss characteristics (upper element: wire).

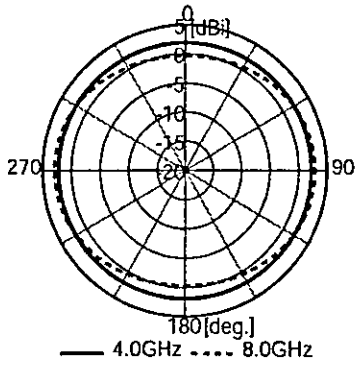

Fig. 14 Radiation characteristics in the horizontal plane (*xy*-plane. upper element: wire).

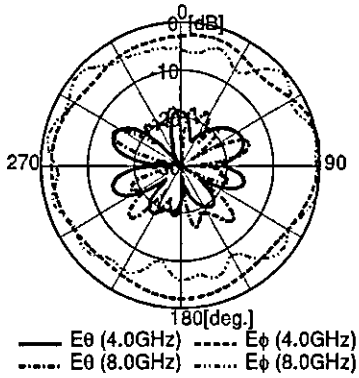

Fig. 15 Radiation characteristics of experimental antenna (*xy*-plane. upper element: wire).

return loss level in the eliminated frequency range was from −3 to almost 0 dB. Either the rectangular element or the wire element could be the upper element to make dual frequency characteristics. This is because the lower resonant frequency is affected by the total antenna size, especially H, and the higher resonant frequency is affected mostly by the lower part, i.e., H_l. The simulated and measured return loss characteristics agree with each other.

Figure 14 shows the simulated radiation characteristics of the antenna. These characteristics are in the horizontal plane with frequencies of 4.0 and 8.0 GHz, respectively. The cross polarization characteristics at each frequency are suppressed to less than −20 dBi (not shown). The measured radiation characteristics are shown in Fig. 15. The simulated and measured radiation patterns agree with each other. Cross polarization characteristics appear in the figure, because the finite ground plane was used for the measurement instead of the infinite ground plane and the cable effect was apparent. From this figure, the radiation patterns at each frequency are similar to that of a monopole antenna, i.e., approximately omni-directional in the horizontal plane. The antenna radiation pattern when using the wire for the upper element is similar to that of the antenna with the upper rectangle. However, there is a small distortion in the radiation patterns at the higher frequency. This is because the antenna's structure is planar; therefore, the radiation from the antenna in the direction in which the antenna is on is different from that in the direction in which the antenna is crossed. To suppress the distortion in the radiation pattern, a three-dimensional structure can be considered in place of a planar structure.

3.5 Current Distribution Characteristics

Figures 16 and 17 respectively show the current distributions of the wire monopole and planar rectangular monopole antennas at each resonant frequency shown in Fig. 2. Although the current magnitude is strong at the feed part, it is suppressed to less than −30 dB at the top of the monopole. The results for the planar rectangular monopole are similar.

So far the analysis shows that the proposed planar monopole antenna has dual frequency characteristics and that a monopole-like radiation pattern can be achieved at both resonant frequencies. Figure 18 shows the current distributions of the antenna at each resonant frequency. Both resonant frequencies are shown in Fig. 5. Figure 18(a) shows the current distribution at the lower resonant frequency and (b) shows the one at the higher resonant frequency.

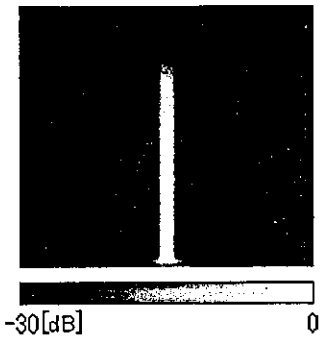

Fig. 16 Current distribution of wire monopole antenna (Freq. = 3.50 [GHz]).

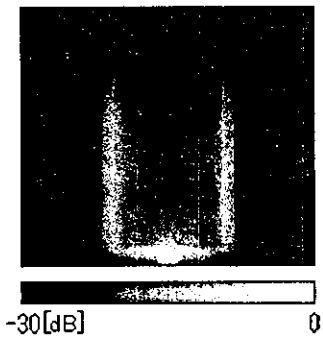

Fig. 17 Current distribution of planar rectangular monopole antenna when W = 12 [mm] (Freq. = 3.85 [GHz]).

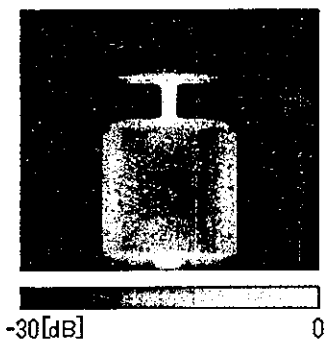

(a) Freq. = 3.32 [GHz]

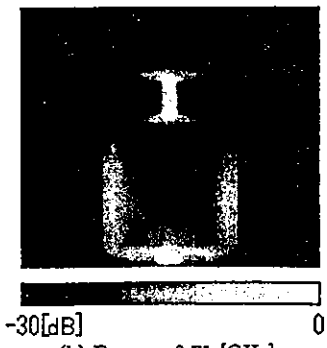

(b) Freq. = 8.71 [GHz]

Fig. 18 Current distribution of dual frequency planar monopole antenna.

At the lower resonant frequency of 3.3 GHz, the magnitude of current is strong at the feed and connector parts. The current distribution at the vertical edges is almost the same as that of a rectangular monopole, and the current level is suppressed to less than −30 dB at the top of the antenna, as shown in Fig. 18(a). From Fig. 18(b), the current level is strong at the feed pin at the higher resonant frequency of 8.7 GHz. The current distribution is similar to that of a rectangular monopole at the vertical edges of the lower rectangle, and the current level is less than −30 dB at the top of the lower rectangle.

These current distribution characteristics indicate that the lower resonant frequency is affected by the total height of the planar monopole antenna, while the higher resonant frequency is affected by the height of the lower rectangle element. This is the same result as gotten from the previous section's return loss characteristics by changing the size of the upper element. The current distributions at each frequency are similar to those of a planar rectangular monopole, so the radiation patterns become omnidirectional in the horizontal plane at each resonant frequency. As a result, a wide bandwidth can be achieved.

4. Orthogonal Planar Monopole Antenna

4.1 Antenna Structure

Figure 19 shows the orthogonal dual frequency planar monopole antenna. This antenna is made by crossing two dual frequency planar monopole antennas identical to that in Fig. 12. The two planar parts are at 90 degrees with respect to each other. Thus, the plate elements of this antenna are orthogonal and are of the same size.

The height of the planar monopole is H and the length of the feed pin is g = 1 mm. The upper rectangular element area is $H_u \times W_u$, and lower one is $H_l \times W_l$. The length of the connector pin between the upper and lower elements is z. Thus, $H = H_u + z + H_l + g$. The upper parts of this planar monopole antenna are wire-like and the lower parts are rectangular. The antenna characteristics were simulated by using the FDTD method. The FDTD parameters were

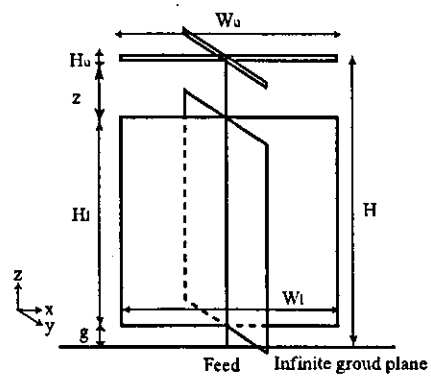

Fig. 19 Analysis model of orthogonal dual frequency planar monopole antenna.

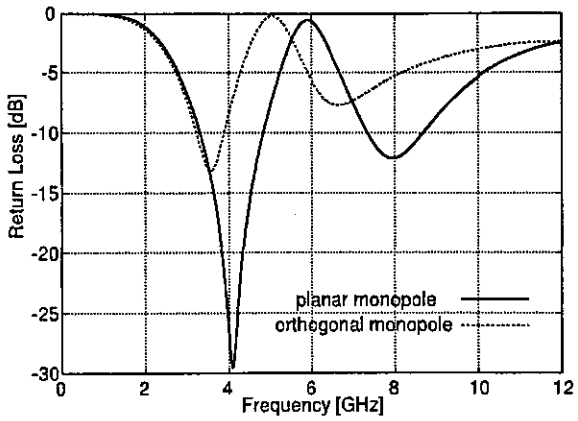

Fig. 20 Return loss characteristics for antenna structures.

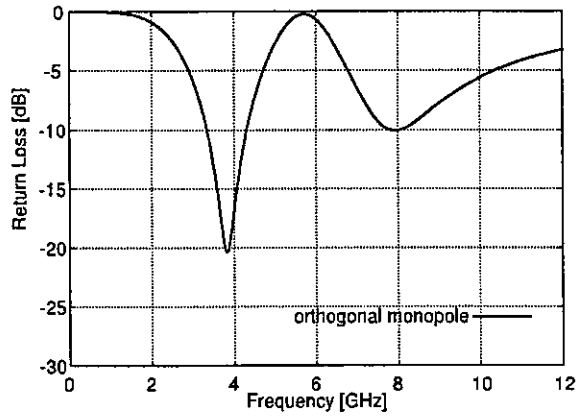

Fig. 21 Return loss characteristics of orthogonal planar monopole antenna.

the same as in Table 1.

4.2 Return Loss Characteristics

The return loss characteristics of the dual frequency planar monopole antenna and novel orthogonal planar monopole antenna, whose analysis models are shown in Figs. 12 and 19 respectively, are compared in this section. The size parameters are the same as in the previous section. The return loss characteristics are shown in Fig. 20. From this figure, it is apparent that the novel orthogonal planar monopole antenna has dual frequency characteristics. The resonant characteristic shifts to a lower frequency range from that of the dual frequency planar monopole because of the electrical antenna's size. At each resonant frequency, this antenna has broadband characteristics. The return loss level is suppressed to less than −6 dB, from about 3 to 4.5 and 6 to 8 GHz for VSWR < 3, but the level increases between both resonant frequencies. The return loss level is more than −3 dB, reaching almost 0 dB, at the eliminated frequencies around 5–6 GHz.

The previous antenna parameters give return loss characteristics that don't cover the required antenna characteristics. In particular, the resonant frequencies should be shifted to a higher frequency to cover the UWB frequency range and eliminate the undesired frequency range. An orthogonal planar monopole antenna with the following parameters was analyzed. The antenna's height and width are H = 17 mm and $W_u = W_l$ = 12 mm. z = 5 mm, H_l = 14 mm, and H_u is infinitesimal (= 0). The return loss characteristics are shown in Fig. 21. This can cover the UWB frequency range and eliminate the undesired frequency range. The return loss characteristic is affected by the antenna's size, as is the case with the dual frequency planar monopole antenna. When the shape of the upper element is rectangular instead of wire-like, similar return loss characteristics to that of using a wire-like structure can be achieved.

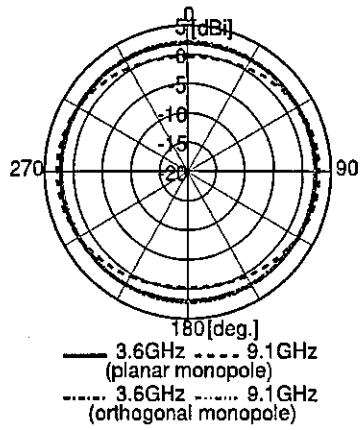

Fig. 22 Radiation characteristics of orthogonal planar monopole antenna in the horizontal plane (xy-plane).

4.3 Radiation Characteristics

Figure 22 shows the radiation characteristics of the orthogonal dual frequency planar monopole antenna and that of the planar dual frequency monopole antenna. These characteristics are in the horizontal plane with respect to 3.6 and 9.1 GHz. The cross polarization characteristics of the antenna at each frequency are suppressed to less than −20 dBi (not shown). From this figure, the radiation patterns at each frequency are similar to that of a monopole antenna, i.e., approximately omni-directional in the horizontal plane. Unlike the radiation pattern of the planar antenna, there is no distortion in the orthogonal planar monopole's radiation pattern. The radiation characteristics are thus improved by using the orthogonal structure. When the shape of the upper element is rectangular instead of wire-like, the similar radiation characteristics to that of using wire-like structure can be achieved.

5. Conclusion

This paper presented two types of planar rectangular monopole antenna. These novel antennas had either a planar structure or an orthogonal structure, and they consisted

of upper and lower elements that were connected. Both can be made by cutting slits into the vertical edges of rectangular planar antennas. The return loss characteristics, radiation pattern and current distribution were simulated by using the FDTD method. Both antennas were shown to have dual frequency and wideband characteristics. The return loss level at the eliminated frequency range between the two resonances was more than −3 dB, reaching almost 0 dB. The radiation patterns over the whole frequency range were almost omni-directional in the horizontal plane. The current distributions were examined, and the characteristics at each frequency were found to be similar to that of a planar rectangular monopole.

References

[1] T. Taniguchi and T. Kobayashi, "An omnidirectional and low-VSWR antenna for ultra-wideband wireless systems," 2002 Radio and Wireless Conf., pp.145–148, Aug. 2002.

[2] N.P. Agrawall, G. Kumar, and K.P. Ray, "Wide-band planar monopole antennas," IEEE Trans. Antennas Propag., vol.46, no.2, pp.294–295, Feb. 1998.

[3] R.C. Comptopm, R.C. McPhedran, Z. Popovic, G.M. Rebeiz, P.P. Tong, and D.B. Rutledge, "Bow-tie antennas on a dielectric half-space: Theory and experiment," IEEE Trans. Antennas Propag., vol.AP-35, no.6, pp.622–631, June 1987.

[4] J.D.S. Langley, P.S. Hall, and P. Newham, "Novel ultrawideband Vivaldi antenna with low crosspolarization," Electron. Lett., vol.29, no.23, pp.2004–2005, Nov. 1993.

[5] M. Hammoud, P. Poey, and F. Colombel, "Matching the input impedance of a broadband disc monopole," Electron. Lett., vol.29, no.4, pp.406–407, Dec. 1993.

[6] Y. Ebine and K. Kagoshima, "Multi-frequency dipole antenna with closed-spaced parasitic elements," IEICE Trans. Commun. (Japanese Edition), vol.J71-B, no.11, pp.1252–1258, Nov. 1988.

[7] Y. Rikuta, H. Arai, and Y. Ebine, "Two-layer antenna with dual frequency," IEICE Trans. Commun. (Japanese Edition), vol.J86-B, no.9, pp.1825–1832, Sept. 2003.

Yuko Rikuta received the B.E., M.E. and Ph.D. degrees in electrical and computer engineering from Yokohama National University, Yokohama, Japan, in 1998, 2000 and 2003, respectively. Currently, she is a research fellow of UWB technology institute in National Institute of Information and Communications Technology. Her research activity and interests are in the area of designing wireless communication antenna. She is a member of the IEEE.

Ryuji Kohno received the Ph.D. degree in electrical engineering from the University of Tokyo in 1984. Since 1998 he is a Professor in the Division of Physics, Electrical and Computer Engineering, Graduate School of Engineering, Yokohama National University (YNU). He has been a president of COE for Creation of Future Social Infrastructure Based on Information Telecommunications Technology in YNU since October 2002. He was a director of Advanced Telecommunications Laboratory of SONY CSL during 1998–2002 and is currently a director of UWB Technology Institute of National Institute of Information and Communications Technology. He was elected as a member of the Board of Governors of IEEE Information Theory (IT) Society in 2000 and 2003. He is an editor of the IEEE Transactions on Communications and that on Intelligent Transport Systems. He was the Chairman of the IEICE Technical Group on Spread Spectrum Technologies, that of Intelligent Transport System and now he is that on Software Radio. He is a chair-in honor of 2002 & 2003 International Conference of Software Defined Radio (SDR'02 & SDR'03), a general co-chair of 2003 IEEE International Symposium on IT (ISIT'03), a general chair of 2004 International Workshop on Ultra Wideband Systems Joint with Conference on Ultra Wideband Systems and Technologies (Joint UWBST & IWUWBS'04), and so on. He was awarded IEICE Greatest Contribution Award and NTT DoCoMo Mobile Science Award in 1999 and 2002, respectively.

Linear maximum likelihood decoding of space – time block coded OFDM systems for mobile communications

G.T.F. de Abreu, H. Ochiai and R. Kohno

Abstract: A new linear decoder for space–time block codes is presented, which enables linear maximum-likelihood decoding in scenarios beyond those described by block-fading models. The new decoder employs linear combinations of received signals with weights designed so as to yield orthogonal estimates for all encoded symbols regardless of channel variations within the block transmission, provided that the channel is known. The combination weights are scalar functions of the channel estimates, obtained through systematic rotations over the decoding matrices of the linear maximum-likelihood decoder for the block-fading case. The proposed decoder yields good performance with low-complexity and is therefore suitable for low-cost portable receivers supporting space–time transmit diversity at the downlink of high data-rate wireless mobile communication systems. Combined with OFDM technology, the technique yields a low-complexity receiver that is effective in combating both time and frequency selectivities, and provides a tool to add flexibility to wireless local area network systems and to offer high data-rate services with support to mobility.

1 Introduction

Orthogonal block space–time transmit diversity, also known as orthogonal space–time block codes (STBCs), has attracted increasing attention since the proposal of the Alamouti scheme [1] and its generalisation by Tarokh [2, 3]. In fact, when combined with maximum ratio combiner (MRC) receive diversity schemes, this technique can transfer a significant amount of the system complexity to the base stations.

Although various space–time codes have since been invented, orthogonal STBCs remain attractive for their excellent balance of performance and low complexity. Orthogonal STBCs were originally developed for high-data-rate systems in flat, block-fading channels, based on the assumptions that symbol rates are much larger than typical fading rates and that frequency selectivity can be neglected. In such channels, a fundamental advantage of the block structure, in comparison to the alternative trellis structure such as those proposed in [4, 5], is the possibility of decoupling symbol estimates thorough simple linear combinations of the received signals, enabling low-complexity symbol-by-symbol maximum likelihood decoding (MLD). This technique, hereafter referred to as linear maximum likelihood decoding (LMLD), was one of the main appeals of Alamouti's original scheme [1] and has been recently generalised [6] to orthogonal space–time block codes of any order [2]. Linear maximum likelihood decoding of orthogonal space–time block codes brings the complexity involved in the application of such codes to implementable levels (even with higher order modulation schemes). Unfortunately, this attractive technique is presently known only for space–time block codes in block-fading channels, which inherently limits its applications to low mobility scenarios.

In the ever more information-hungry modern and future societies, however, high-data-rate services are demanded not only by stationary users, but also by users on the move. A prominent example of practical interest is public wireless local area networks (WLANs) increasingly found in public places such as airports and train stations, and utilised by people moving at different speeds, on foot and travelators, as well as bicycles, karts and shuttles. Another is private WLANs supporting seamless indoor–outdoor transitions so as to serve users not only inside buildings but also outside.

However, in such systems with support for moderate mobility, the effect of time-varying frequency selectivity over space–time code structures cannot be neglected. In a single-carrier high-data-rate wireless system applying STBCs, for instance, frequency selectivity causes encoded blocks to overlap with random delays. The resulting intersymbol interference (ISI) destroys the orthogonality of the code and impedes (conventional) linear maximum likelihood decoding.

Fortunately, frequency selectivity can be effectively mitigated with orthogonal frequency-division multiplexed (OFDM) technology [7]. Nevertheless, there are intrinsic characteristics of OFDM systems that make the introduction of space–time block codes into such systems less straightforward than might be expected at first glance. For instance, the symbol periods in OFDM systems are much longer than that of a single-carrier system with the same data-rate, such that a fading process slow enough to be considered block-fading in a single carrier system, might not be so in a system with an OFDM architecture. Similarly, in the frequency domain, implementation issues limit the total

IEE Proceedings online no. 20040663

doi:10.1049/ip-com:20040663

Paper first received 15th August 2003 and in revised form 19th April 2004. Originally published online: 1st July 2004

G.T.F. de Abreu is with the Centre for Wireless Communications, University of Oulu, P.O. box 4500, 90014-Oulu, Finland

H. Ochiai and R. Kohno are with the Graduate School of Engineering, Division of Physics, Electrical and Computer Engineering, Yokohama National University, 79-5 Hodogaya, Yokohama, 240-8500 Japan

number of carriers of OFDM systems so that adjacent carriers are still significantly separated, which implies that 'space–frequency' implementations of space–time coding techniques (as suggested in [8]) are also subject to a departure from the original assumption of a quasi-static channel. To summarise, there are applications when neither in the time nor in the frequency domains, can the OFDM channel be considered quasi-static so as to support a straightforward implementation of space–time block codes.

Aiming at combining the advantages of OFDM and STBCs (with LMLD), so as to design low-cost high-data-rate wireless communication systems with support for mobility, applications of the Alamouti scheme to OFDM systems were investigated in [8–11]. Due to the fact that OFDM channels are not quasi-static, the results reported in [8–11] were, however, less than satisfactory. Indeed, it was observed that the bit error rate performances of space–time block encoded OFDM systems saturated (reached error floors) at higher signal-to-noise ratios. The same conclusion was reached in a previous work where the Alamouti scheme was applied in a non-block-fading channel [12], tracked with a (computationally costly!) Kalman filter.

What went unnoticed in all such works (i.e., [8–12] and their like), is that the error floors at high signal-to-noise ratios observed with STBCs in non-quasi-static fading channels are not an intrinsic problem of the codes, but a consequence of inadequate decoding. In fact, strict MLD is theoretically always possible (see [3]), at the price of a higher complexity (although this alternative is in most cases prohibitively complex).

In additional to the low decoding complexity involved, there are other good reasons that stimulate us to consider LML decoded STBCs for low-cost, portable receivers in mobile wireless OFDM systems in urban environments (with moderate, yet non-block, fading channels). For instance, highly accurate, low-complexity, two-dimensional channel estimation techniques are available [13–15] for OFDM systems in these scenarios. Since decoding orthogonal STBCs is essentially a coherent process and as such, dependent on the accuracy of channel estimation, this property of OFDM systems highly favour STBCs as opposed to space–time trellis codes. In fact, while the fading processes typically faced by mobile wireless OFDM systems in urban environments is fast enough to impair the introduction of (non-coherent) differential space–time block coding [16, 17], these are not fast enough to favour the use of more complex trellis-based space–time diversity methods [4, 5], which are, in general the best fit for fast-fading channels. Finally, unlike the latter, STBCs with LMLD enable real-time decoding of transmitted signals, required by some applications.

2 Channel model

Consider an M-carrier OFDM system with bandwidth B and center frequency f_C in a multipath mobile wireless channel with delay spread $\Delta\tau$. The complex baseband representation of such a channel is given by

$$h(t) = \sum_k \gamma_k(t)\delta(t-\tau_k) \tag{1}$$

where $\gamma_k(t)$ and τ_k are the complex amplitude and the normalised delay of the kth path, respectively.

Owing to motion, $\gamma_k(t)$ are wide-sense stationary complex gaussian processes, independent for each k . In addition, both their average power σ_k^2, and probability of occurrence, decay exponentially with τ_k [18].

If v is the relative speed between transmitter and receiver, the Doppler spread at the mth carrier is given by

$$f_D(m) = \frac{v}{c}\left(m\frac{B}{M-1} + f_C - \frac{B}{2}\right) \tag{2}$$

where $m = 0, \ldots, M-1$.

Typically, however, $B \ll f_C$ and $f_C \gg 0$ that $f_D(m)$ can be considered the same at all carriers. The time varying frequency response of the channel, $H(t, f)$, can then be written as

$$H(t,f) = \sum_k \gamma_k(t)e^{-j2\pi f\tau_k} \tag{3}$$

The two-dimensional complex fading process $H(t,f)$ has an envelope autocorrelation well approximated by [19]

$$R_H(\Delta t, \Delta f) = \sigma_H^2 \frac{J_0^2(2\pi\Delta t f_D)}{1+(2\pi\Delta\tau\Delta f)^2} \tag{4}$$

where σ_H^2 is the total average power of the channel and $J_0(\cdot)$ is the 0th order Bessel function of the first kind. An illustrative example of channels with this description is shown in Fig. 1.

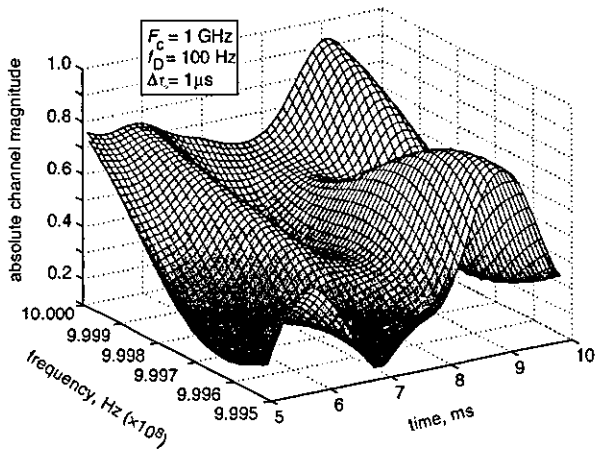

Fig. 1 *Typical OFDM channel through a 500 ms-by-500 kHz window*

It is known that the two-dimensional autocorrelation envelope of the time and frequency fading processes observed in the OFDM channel given by (4) can be separated if the normalised autocorrelation functions of all $\gamma_k(t)$ are the same [14]. In this case it can be shown that [19]

$$R_H(\Delta t, \Delta f) = \sigma_H^2 R_t(\Delta t) R_f(\Delta f) \tag{5}$$

where

$$R_t(\Delta t) = J_0(2\pi\Delta t f_D) \tag{6}$$

$$R_f(\Delta f) = \frac{J_0(2\pi\Delta t f_D)}{1+(2\pi\Delta\tau\Delta f)^2} \tag{7}$$

Comparing (1) and (3) we observe that for any given carrier f_m, the processes $h(t)$ and $H(t,f_m)$ have similar statistics, since the terms $e^{-j2\pi f_m\tau_k}$ only affect the phases of $\gamma_k(t)$. Indeed, in both cases, $R_t(\Delta t)$ is parameterised only by the Doppler spread f_D. In other words, the time-domain fading process observed at each carrier of an OFDM system is equivalent to that observed in a low-data-rate single-carrier system.

On the other hand, for a fixed instant t, all $\gamma_k(t)$ are constant, so that the frequency-domain fading process depends on the instantaneous distribution of the

magnitudes of $\gamma_k(t)$. The fading observed across the carriers in an OFDM system is therefore not the same as the time-domain fading process observed in narrowband single-carrier systems, despite having the same (Rayleigh) distribution. This is rather evident from the fact that the autocorrelation function $R_f(\Delta f)$ is parameterised both by the Doppler f_D spread and the delay spread $\Delta\tau$.

As an illustration to the fact that a typical OFDM channel is not accurately described by a block-fading model, consider the downlink of a wireless system operating at the 5 GHz band towards a mobile with relative speed of 11 km/h, so that the Doppler frequency spread experienced is 50 Hz.

If the system is single-carrier and transmits symbols taken from an 8PSK constellation with a data-rate of 10 Mbit/s, the symbol period is of approximately 0.3 μs. Assuming Rayleigh fading, this means that the autocorrelation of channel samples taken every, say, 100 symbols is virtually 1. In other words, the channel is quasi-static and the block-fading assumption holds.

However, in a typical urban environment with a delay spread of 3 μs [18], the single carrier system employing STBC will experience intersymbol interference. Suppose that in order to combat intersymbol interference a 512-carrier OFDM system is set up. The symbol period in this system is approximately 0.1536 ms and the carrier separation will be around 6.5 kHz. In this case, the normalised time domain autocorrelation of channel samples taken at every symbol drops to 0.9999. This figure indicates that the channel can be considered constant over the transmission of a symbol. Over the transmission of an eight-symbol long STBC, e.g. $\boldsymbol{G}_3$ and $\boldsymbol{G}_4$, the figure falls to 0.9907 and for samples taken every 16 symbols (block-length of codes $\boldsymbol{G}_5$–$\boldsymbol{G}_8$) the number is 0.9631. Similarly, while the autocorrelation of channel samples taken at every carrier is 1, the figure drops to 0.9976 for samples taken every 8 carriers, and to 0.9903 for samples taken every 16 carriers.

In other words, even in typical urban channels with relatively small Doppler frequencies and moderate delay spreads, the fading experienced by OFDM signals is slightly (yet not negligibly) different in both the time domain (from symbol to symbol) and the frequency (from carrier to carrier) domain.

Two important things are learned from the numerical example given above. The first is that typical channel variations are still slow enough that the channel can be considered constant over a symbol. This implies that the problem of co-channel (carrier-to-carrier) interference due to symbol distortion can be neglected (in fact dealt with independently) when considering decoding of STBCs in OFDM systems. The second is that while smooth channel variation is observed across a block of a few symbols, this is typically not strong enough to favour space–time diversity methods designed for the fast-fading scenario.

Given the above discussion, the model used throughout this paper to describe the fading process faced by OFDM signals in the time (across successive symbols) and frequency (across adjacent carriers) domains is that of highly correlated, symbol-by-symbol and carrier-by-carrier Rayleigh fading. The accuracy of this model is further enforced by the fact that a guard interval between consecutive symbols is commonly use in OFDM systems.

In the following, it will also be assumed that the channels observed across different transmit antennas (space domain) are statistically independent and identically distributed (IID).

3 Decoding of Alamouti STBC in non-quasi-static channels

Block space–time diversity schemes in OFDM systems can be applied both in space–time and space–frequency arrangements. In a space–time arrangement, the STBC structure is applied independently at each carrier, so that codewords are transmitted over a number of transmit intervals. In a space–frequency arrangement, codewords are transmitted over a number of adjacent carriers simultaneously, so that at each transmit interval a new coded block is transmitted.

It was shown in [11] and [8] that depending on channel conditions (determined by the delay spread $\Delta\tau$ and the Doppler frequency f_D) and on system parameters such as the symbol period Δt and the distance between adjacent carriers Δf, one arrangement might yield better results than the other. These works show that in fact these two arrangements are equivalent in the sense that the performances of the space–time and space–frequency arrangements in a certain channel are equivalent to those of corresponding space–frequency and space–time arrangements in another channel where the fading processes in frequency and time domains have inverted properties. For these reasons we shall hereafter, without loss of generality, use notation and language only based on a space–time framework, i.e., assuming that the STBC is applied to every carrier using N-transmit antennas. It is clear that the results hold also for OFDM systems employing space–time codes in a space–frequency arrangement.

3.1 Conventional combiner

Let S_i denote the data symbol transmitted by the ith transmit antenna (through any arbitrary carrier) and $H_i[t]$ its channel state at the tth time interval.

As discussed in Section the preceding, it is assumed that $H_i[t]$ is constant during the transmission of S_i, but changes to $H_i[t+1]$ at the next transmit interval. In this case, the received signals at times t and $t+1$ become

$$Y[t] = H_1[t]S_1 + H_2[t]S_2 + W[t] \tag{8}$$

$$Y[t+1] = H_2[t+1]S_1^* - H_1[t+1]S_2^* + W[t+1] \tag{9}$$

where W denotes zero-mean random white Gaussian complex noise with independent in-phase and quadrature components each with variance $\sigma^2_{W/2}$.

Assuming that the channel is perfectly estimated, the question that arises is what combination of received signals and channel values must be used in order to obtain orthogonal estimates of S_i.

In previous works [8–12], the difference between $H_i[t]$ and $H_i[t+1]$ is neglected and the pairs $(H_1[t]^*, H_2[t])$ and $(H_2[t]^*, -H_1[t])$ are used to combine the received signals for estimates of the transmit symbols, resulting in:

$$\begin{aligned}\hat{S}_1 &= H_1[t]^* Y[t] + H_2[t]Y[t+1]^* \\ &= (|H_1[t]|^2 + H_2[t]H_2[t+1]^*)S_1 + H_2[t](H_1[t]^* \\ &\quad - H_1[t+1]^*)S_2 + W[t]H_1[t]^* + W[t+1]^*H_2[t]\end{aligned} \tag{10}$$

$$\begin{aligned}\hat{S}_2 &= H_2[t]^* Y[t] - H_1[t]Y[t+1]^* \\ &= (|H_2[t]|^2 + H_1[t]H_1[t+1]^*)S_2 + H_1[t](H_2[t]^* \\ &\quad - H_2[t+1]^*)S_1 + W[t]H_2[t]^* - W[t+1]^*H_1[t]\end{aligned} \tag{11}$$

This is equivalent to what a system designed for the block-fading channel and employing the Alamouti scheme would obtain as estimates in the presence of a non-quasi-stationary fading process. Equations (10) and (11) clearly show that if the channel values vary slightly from one transmission instant to the other ($H_1[t] \neq H_1[t+1]$), the estimates obtained with the conventional linear decoder for Alamouti's scheme are (strictly) no longer orthogonal.

Let us quantify the average effect, in terms of intrasymbol interference, that is caused by such a block-fading-oriented decoding in the presence of a non-quasi-static fading channel. Assuming that the fading rate is not too fast, consecutive samples of the same process can be related by an auto-regressive model [12]

$$H_i[t+1] = \alpha_i H_i[t] + V_i[t] \tag{12}$$

where V_i are zero-mean complex Gaussian random variables uncorrelated to H_i, and α_i is given by

$$\alpha_i = \frac{E[H_i[t]H_i[t+1]^*]}{\sigma_{H_i}^2} = R_t(\Delta t) = J_0(2\pi\Delta t f_D) \tag{13}$$

In the equation above, $E[\cdot]$ denotes the expected value, $\sigma_{H_i}^2$ the variance (power) of the ith diversity branch H_i and Δt is the time lag between successive transmissions at t and $t+1$, that is, the symbol period.

Strictly speaking, α_i take complex values. However, if the channel variation from instant t to $t+1$ is not too fast, α_i have very small phase and can be approximated by real numbers [19]. Then, the following approximation holds:

$$E\left[\left|H_i[t]\right|^2 + H_j[t]H_j[t+1]^*\right] \approx (\sigma_{H_i}^2 + J_0(2\pi\Delta t f_D)\sigma_{H_j}^2) \tag{14}$$

Next, define the normalised interference coefficient ρ_i as the average of the absolute value of the ith channel variation from $H_i[t]$ to $H_i[t+1]$:

$$\rho_i = \sqrt{\frac{(E[|H_i[t] - H_i[t+1]|])^2}{\sigma_{H_i}^2}} \tag{15}$$

The coefficient that multiplies the interfering symbol S_j in the estimate of S_i then becomes:

$$E\left[\left|H_j[t](H_i[t] - H_i[t+1])^*\right|\right] = \sigma_{H_i}\rho_i E\left[\left|H_j[t]\right|\right] \tag{16}$$

Since $E\left[\left|H_j[t]\right|\right]$ is simply the average value of a Rayleigh random variable, we finally have [20]

$$E\left[\left|H_j[t](H_i[t] - H_i[t+1])^*\right|\right] = \sigma_{H_i}\rho_i\sigma_{H_j}\Gamma\left(\frac{3}{2}\right) \tag{17}$$

The coefficients ρ_i are clearly dependent on the speed with which the channel varies from symbol to symbol (fading rate), which can be measured by the autocorrelation of the channel. In order to simplify the notation it is hereafter assumed that the diversity branches are balanced, i.e., $\sigma_{H_1}^2 = \sigma_{H_2}^2 = \sigma_H^2$, so that the subscript i can be dropped from α_i and ρ_i.

Expanding (15) and using the approximation given in (14), the following is obtained for Rayleigh fading channels with variance σ_H^2 and the normalised autocorrelation function given by (6):

$$\rho = \sqrt{2(1-\alpha)} \tag{18}$$

Although it was assumed that the channel $H_i[t]$ varies slightly to $H_i[t+1]$, it is found that (18) accurately models the relationship between the interference coefficient ρ and the autocorrelation of the channel even for higher fading rates. Figure 2 illustrates this fact comparing results

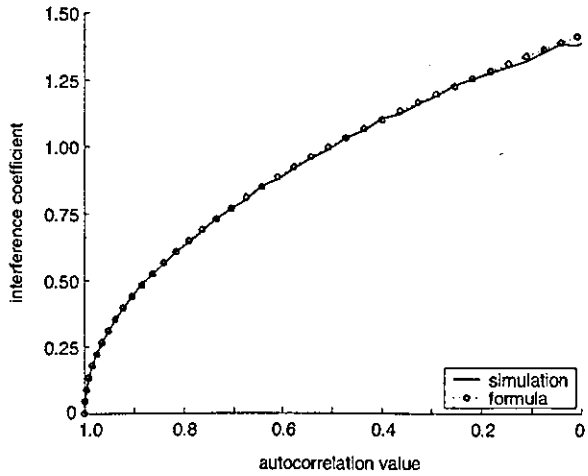

Fig. 2 *Variation of the normalised interference coefficient against the channel normalised autocorrelation*

obtained with (18) to those obtained directly from (15) through computer simulations.

It is noticeable from Fig. 2 that ρ grows quickly even for small deviations from the ideal autocorrelation $\alpha = 1$ (corresponding to a perfect block-fading channel). This implies that in a channel that is slightly non-block-fading, significant intrasymbol interference is caused by the linear combiner described through equations (10) and (11).

Indeed, the performance of the STBC in a non-quasi-static fading channel with balanced diversity branches is driven by the following average signal-to-interference-plus-noise ratio (SINR)

$$\xi = \frac{(1 + J_0(2\pi\Delta t f_D))\sigma_H^2\sigma_S^2}{2\sigma_W^2 + \sqrt{2(1 - J_0(2\pi\Delta t f_D))}\Gamma\left(\frac{3}{2}\right)\sigma_H^2\sigma_S^2} \tag{19}$$

where σ_S^2 is the average energy of the transmit symbols (energy of the signal constellation).

While the diversity order achieved by the code is given by $(1 + J_0(2\pi\Delta t f_D)) \leq 2$, the denominator term $\sqrt{2(1 - J_0(2\pi\Delta t f_D))}\Gamma(1.5)$ in the denominator accounts for the orthogonality loss caused by the inadequacy of the decoder facing a non-block-fading channel. In noisy scenarios ($\sigma_W^2 \geq \sigma_S^2$), or in channels with absolutely no variation within blocks ($\rho = 0$) (19) reduces to

$$\xi = \frac{\sigma_H^2\sigma_S^2}{\sigma_W^2} \tag{20}$$

Equation (20) indicates that, in noisy non-block-fading channels, the Alamouti space–time diversity scheme with the above decoder performs approximately as well as in a block-fading channel.

In typical OFDM systems however, the channel is non-quasi-static ($\rho \neq 0$) and the case of practical interest for high-data-rate wireless mobile communication is that of a low-noise scenario ($\sigma_W^2 < \sigma_S^2$). In this case, a floor on the SINR inversely proportional to the term $\sqrt{2(1 - J_0(2\pi\Delta t f_D))}\Gamma(1.5)$ is reached. This indicates that there is a signal-to-noise-ratio beyond which no improvement is observed on the bit error rate performance of the space–time coded OFDM system, as observed in [8–11]. Identical results are obtained if the pair of channel states $(H_1[t+1]^*, H_2[t+1])$ and $(H_2[t+1]^*, -H_1[t+1])$ are respectively used to obtain estimates for S_1 and S_2.

Taking another look at (10) and (11) we see that if the fading rate is too fast that $E[H_i[t]H_i[t+1]^*] = 0$, ρ reduces to $\sigma_H\sqrt{2}$ and $E\left[\left||H_i[t]|^2 + H_j[t]H_j[t+1]^*\right|\right]$ to σ_H^2. Consequently, the diversity order deteriorates to 1 (no diversity gain), and the interference increases to a maximum level of $\sqrt{2}\Gamma(1.5)$. In this case, the SINR becomes:

$$\xi = \frac{\sigma_H^2\sigma_S^2}{2\sigma_W^2 + \sqrt{2}\Gamma\left(\frac{3}{2}\right)\sigma_H^2\sigma_S^2} \tag{21}$$

This scenario corresponds to the Alamouti scheme in a fast fading environment. We emphasise that this analysis is purely illustrative since, if the fading rate is that high, channel estimation itself would represent a difficult problem, not to mention that channel variation within the transmission of a symbol (which is a cause of co-channel interference in OFDM systems) could not be neglected. Equation (21), however, is helpful to illustrate why linear combining is no longer effective if STBCs are used in fast fading channels. In fact, it is known that in fast-fading channels other space–time coding techniques, which nevertheless require more complex maximum likelihood decoding, outperform STBCs [4].

Fast-fading channels, which are related to very high mobile speeds and low carrier frequencies, are not typical in OFDM systems, but can be artificially created by the use of interleaving. However, in typical urban scenarios with small Doppler frequencies, very long interleavers would be required in order for fast-fading space–time codes to yield significant gain, at the cost of higher complexity and sacrificing real-time decoding.

In contrast, the technique presented in this paper is aimed at enabling real-time, low-complexity (symbol-by-symbol) maximum likelihood decoding of orthogonal STB coded OFDM systems in typical non-quasi-static (yet not fast) fading channels. The analysis and application of space–time coding schemes to OFDM systems in fast-fading scenarios are therefore out of the scope of this work.

3.2 Maximum diversity combiner

Alternatively to the conventional combiner shown in the previous subsection, $(H_1[t]^*, H_2[t+1])$ and $(H_2[t]^*, -H_1[t+1])$ could be respectively used to obtain estimates for S_1 and S_2, ensuring that the maximum diversity order is achieved. In this case we have:

$$\begin{aligned}\hat{S}_1 =& H_1[t]^*Y[t] + H_2[t+1]Y[t+1]^* \\ =& (|H_1[t]|^2 + |H_2[t+1]|^2)S_1 + (H_2[t]H_1[t]^* \\ & - H_2[t+1]H_1[t+1]^*)S_2 + W[t]H_1[t]^* \\ & + W[t+1]^*H_2[t+1]\end{aligned} \tag{22}$$

$$\begin{aligned}\hat{S}_2 =& H_2[t]^*Y[t] - H_1[t+1]Y[t+1]^* \\ =& (|H_1[t+1]|^2 + |H_2[t]|^2)S_2 + (H_1[t]H_2[t]^* \\ & - H_1[t+1]H_2[t+1]^*)S_1 + W[t]H_2[t]^* \\ & - W[t+1]^*H_1[t+1]\end{aligned} \tag{23}$$

If $H_i[t]$ and $H_j[t]$ are uncorrelated, zero-mean, complex Gaussian processes with variances $\sigma_{H_i}^2$ and $\sigma_{H_j}^2$, respectively, the process $H_i[t]H_j[t]^*$ is also a zero-mean complex Gaussian process with variance $\sigma_{H_i}^2\sigma_{H_j}^2$. Therefore, we have:

$$\begin{aligned}& E\left[|H_i[t]H_j[t]^* - H_i[t+1]H_j[t+1]^*|\right] \\ &= \sigma_{H_i}\sigma_{H_j}\sqrt{2(1 - J_0(2\pi\Delta t f_D))}\end{aligned} \tag{24}$$

Again, for balanced diversity branches, the average SINR resulting from the use of this combiner is given by:

$$\xi = \frac{2\sigma_H^2\sigma_S^2}{2\sigma_W^2 + \sqrt{2(1 - J_0(2\pi\Delta t f_D))}\sigma_H^2\sigma_S^2} \tag{25}$$

Equation (25) means that although full diversity is achieved, this decoder is also not orthogonal in the presence of a non-block-fading channel. In addition, with this combiner, an even larger amount of intrasymbol interference is observed since the factor $\Gamma(1.5) \approx 0.886$ is no longer in the denominator of the SINR formula. Consequently, higher error floors on the bit-error-rate curves will also be observed at the low noise region.

3.3 Orthogonal combiner

From the results obtained with the analysis shown in Sections 3.1 and 3.2, we infer that pursuing a combiner that delivers maximum diversity is not necessarily the right approach in a non-block-fading channel.

Let us combine $Y[t]$ and $Y[t+1]$ using the pairs $(H_1[t+1]^*, H_2[t])$ and $(H_2[t+1]^*, -H_1[t])$, to obtain $\hat{S}_1$ and $\hat{S}_2$, respectively. In this case we have:

$$\begin{aligned}\hat{S}_1 =& (H_1[t]H_1[t+1]^* + H_2[t]H_2[t+1]^*)S_1 \\ & + W[t]H_1[t+1]^* + W[t+1]^*H_2[t]\end{aligned} \tag{26}$$

$$\begin{aligned}\hat{S}_2 =& (H_1[t]H_1[t+1]^* + H_2[t]H_2[t+1]^*)S_2 \\ & + W[t]H_2[t+1]^* - W[t+1]^*H_1[t]\end{aligned} \tag{27}$$

Unlike all the methods above, this combiner is capable of completely decoupling the estimates $\hat{S}_1$ and $\hat{S}_2$, regardless of the values of H_i. As before, in case the fading process is slow enough, the average signal-to-noise-ratio (SNR) obtained becomes:

$$\xi = \frac{2J_0(2\pi\Delta t f_D)\sigma_H^2\sigma_S^2}{2\sigma_W^2} \tag{28}$$

Equation (28) suggests that the full orthogonality provided with this decoder comes at the expense of reducing the diversity order achieved, which is given by $2J_0(2\pi\Delta t f_D)$, clearly less than 2 for $f_D \neq 0$. In a block-fading scenario ($\Delta t f_D \approx 0$) however, as with all other methods above, this combiner reduces to the conventional (maximum-ratio-like) linear combiner for Alamouti's code [1].

In all the linear combiners discussed here, estimates for the symbols S_1 and S_2 are first obtained and then compared to the Q symbols of the transmit constellation. Therefore, the order of complexity of the corresponding decoders is $O(2Q)$.

In contrast, with strict maximum likelihood decoding, no decoupled estimates of the transmit symbols are computed. Instead, decoding is based on the computation of the metric given below, for all possible pairs of S_1 and S_2 in the constellation, which gives a decoding complexity in the order of $O(Q^2)$.

$$\begin{aligned}D_2 =& |Y[t] - (H_1[t]S_1 + H_2[t]S_2)|^2 + |Y[t+1] \\ & - (H_2[t+1]S_1^* - H_1[t+1]S_2^*)|^2\end{aligned} \tag{29}$$

In order to illustrate the difference in terms of complexity, consider that an 8PSK constellation is used. Decoding a pair of symbols with strict maximum likelihood requires the computation of 64 metrics. In contrast, any of the linear decoders discussed in this Section requires only 16 comparisons. In other words, linear decoders maintain the complexity of the coded systems at the same level of

maximum likelihood coherent detection of uncoded systems.

3.4 Performance and complexity

In Fig. 3, the performances of the Alamouti scheme with each of the three linear combiners discussed in this section are compared to that obtained with a strict maximum likelihood decoder. The plot shows the bit-error rate at one of the 1024 carriers of an OFDM system transmitting 8PSK symbols with a nominal data rate of 10 Mbit/s in a channel with a Doppler spread of 75 Hz. Given these parameters, each carrier transmits at about 10 kbit/s and the symbol period is around 0.3 ms so that the normalised autocorrelation of the channel sampled at the symbol rate is approximately 0.9948 (see (6)).

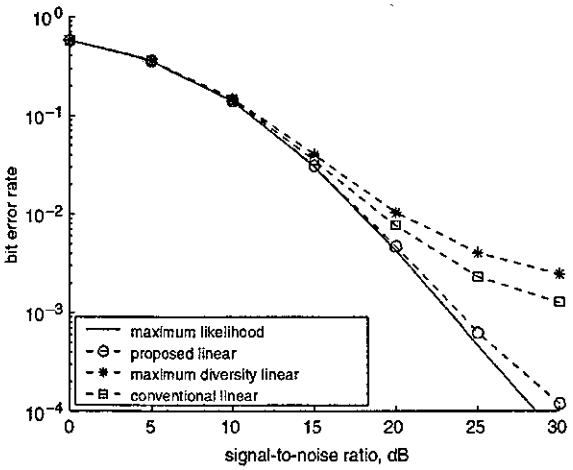

Fig. 3 *Performance of Alamouti scheme (3 bit/s/Hz) in a 1024-carrier OFDM system with 8PSK modulation*
Doppler spread $f_D = 75$ Hz

It is noticeable that the maximum diversity combiner of Sub-section 3.2 performs worse than the conventional combiner of Sub-section 3.1. This result is in accordance with the theoretical analysis given in this Section.

The plot also shows that both the maximum diversity and the conventional (block-fading) decoders exhibit error floors at high SNRs. In contrast, it is seen that the proposed orthogonal linear combiner, which enables symbol-by-symbol maximum likelihood decoding, yields a performance nearly as good as the strict maximum likelihood decoder [3], with no error floor.

On the one hand, the complexity of a strict maximum likelihood decoder for the Alamouti scheme grows with the square of the cardinality of the modulation constellation. On the other hand, higher order modulations imply longer symbols which, for a fixed Doppler spread, result in more interference with the conventional and maximum diversity linear combiners.

This means that the gain of the orthogonal method, in terms of performance enhancement over the other linear combiners, and in terms of complexity reduction over the strict maximum likelihood decoder, is more significant for higher-order modulations.

This fact is illustrated in Fig. 4 where the performances of the Alamouti scheme in the same channel described above but for 10 Mbit/s 1024-carrier OFDM systems with several different modulations are compared.

It is seen that both with the conventional and with the maximum diversity linear combiners, the higher the order of

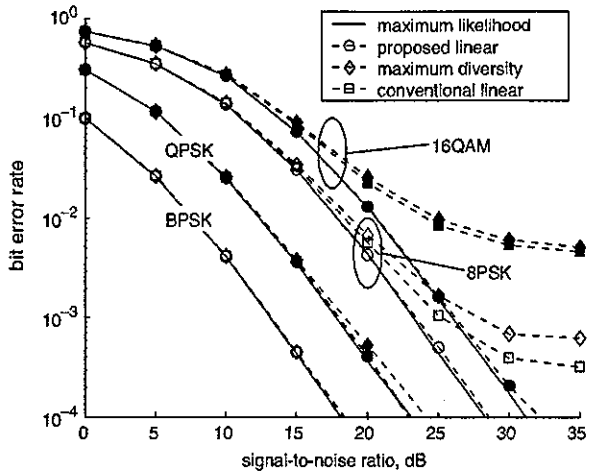

Fig. 4 *Performance of Alamouti scheme (1–4 bit/s/Hz) in a 1024-carrier OFDM system with different modulation schemes*
Doppler spread $f_D = 75$ Hz

the modulation scheme, the higher the error floor reached and the lower the signal-to-noise ratio from where it is established. In contrast, the performance achieved with the orthogonal combiner and symbol-by-symbol maximum likelihood decoding is clearly comparable to that obtained with a strict maximum likelihood decoder.

Note that, for instance, in the case of a 16 QAM constellation, the strict maximum likelihood decoder requires as much as 256 metric-computations in order to decode a single block of two symbols, against only 32 needed with the proposed method! It is also seen that the maximum diversity linear combiner performs slightly worse than the conventional linear combiner.

All the analysis presented here suggests that if low-complexity (linear) maximum likelihood decoding of STBCs in non-quasi-static fading channels is desired, diversity order must be sacrificed in favour of orthogonality. In the following Section we will show that this is the case not only for Alamouti's code but also for Tarokh's generalised STBCs from orthogonal designs [2].

4 Decoding of orthogonal space–time block codes in non-quasi-static channels

The linear orthogonal decoder given in Section 3.3 is restricted to Alamouti's STBC [1]. Although this particular code is known to be the only full rate orthogonal STBC that achieves and full diversity over any complex constellation, the result would be incomplete and less important if not applicable to the generalised STBCs from orthogonal designs developed by Tarokh [2, 3].

In fact, although these generalized orthogonal STBCs have reduced rate, it has been shown [21, 22] that they can be combined to form quasi-orthogonal constructions which, together with constellation rotations techniques [23, 24], yield codes with improved performances.

For the above reasons, we are stimulated to extend the above orthogonal linear decoder for Alamouti's scheme in non-quasi-static fading channels to Tarokh's codes under the same conditions.

4.1 Linear decoding based on a squaring method

In this Section, the squaring method proposed in [6] for linearly decoding generalised orthogonal STBCs in

block-fading is extended to the non-quasi-static fading channel. In order to maintain the notation as simple as possible, and without loss of generality, we consider one-receive antenna, N-transmit antenna schemes. The extension to the case of multiple receive antennas is straightforward.

Consider that an orthogonal STBC is applied to a carrier using N transmit antennas. Let $\boldsymbol{G}_N$ and $\boldsymbol{S}$ denote the code's orthogonal design matrix and a symbol vector constructed with the set of K transmit symbols $(S_1, \cdots, S_K)$ followed by their complex conjugates, as shown in (31).

$$\boldsymbol{G}_N = \begin{bmatrix} c_{1,1} & \cdots & c_{1,n} & \cdots & c_{1,N} \\ \vdots & \ddots & \vdots & \ddots & \vdots \\ c_{k,1} & \cdots & c_{k,n} & \cdots & c_{k,N} \\ \vdots & \ddots & \vdots & \ddots & \vdots \\ c_{2K,1} & \cdots & c_{2K,n} & \cdots & c_{2K,N} \end{bmatrix} \tag{30}$$

$$\boldsymbol{S} = [S_1 \quad \cdots \quad S_K \quad S_1^* \quad \cdots \quad S_K^*]^T \tag{31}$$

In STBCs from orthogonal designs [2], every entry $c_{n,k}$ of $\boldsymbol{G}_N$ is an element of $\boldsymbol{S}$ multiplied by $+1$ or -1, such that the rows of $\boldsymbol{G}_N$ are orthogonal.

Let $\boldsymbol{H}$ and $\boldsymbol{Y}$ denote the channel matrix and the received signal vector, respectively.

$$\boldsymbol{H} = \begin{bmatrix} H_1[t] & \cdots & H_1[t+k] & \cdots & H_1[t+2K-1] \\ \vdots & \ddots & \vdots & \ddots & \vdots \\ H_n[t] & \cdots & H_n[t+k] & \cdots & H_n[t+2K-1] \\ \vdots & \ddots & \vdots & \ddots & \vdots \\ H_N[t] & \cdots & H_N[t+k] & \cdots & H_N[t+2K-1] \end{bmatrix} \tag{32}$$

$$\boldsymbol{Y} = [Y[t] \quad \cdots \quad Y[t+2K-1]] \tag{33}$$

The nth row of $\boldsymbol{H}$ consists of time samples of the continuous fading process corresponding to the nth transmit interval, while the kth row corresponds to the spatial samples of these fading processes across the elements of the transmit array of antennas. In other words, in the context of this paper, it is assumed that $H_n[t+k]$ varies slowly with k (along the columns of $\boldsymbol{H}$), and quickly with n (along its rows).

The received signals are simply the diagonal entries of the product $\boldsymbol{G}_N \cdot \boldsymbol{H}$ plus a noise vector $\boldsymbol{W}$.

$$\boldsymbol{Y} = \mathbf{diag}[\boldsymbol{G}_N \cdot \boldsymbol{H}] + \boldsymbol{W} \tag{34}$$

A squared matrix, analogous to that derived in [6], suitable for linear decoding of STBCs in non-quasi-static fading channels is then obtained by finding a matrix $\boldsymbol{R}$ such that:

$$\mathbf{diag}[\boldsymbol{G}_N \cdot \boldsymbol{H}] = \boldsymbol{R} \cdot \boldsymbol{S} \tag{35}$$

Next, define a vector $\boldsymbol{P}$ constructed with combinations of the received signals and the entries of $\boldsymbol{R}$:

$$\boldsymbol{P} = \boldsymbol{Y} \cdot \boldsymbol{R}^* \tag{36}$$

Then, an estimate $\hat{S}_k$ for the kth transmit symbol S_k is obtained by summing the kth element of $\boldsymbol{P}$ with the complex conjugate of its $(k+K)$th element:

$$\hat{S}_k = \boldsymbol{P}_k + \boldsymbol{P}_{(k+K)}^* \tag{37}$$

If the K different symbols in each block belong to a constellation of cardinality Q, the block is decoded by computing K symbol estimates (37) and then searching the alphabet for those that hold the shortest distance to each estimate. This process involves computing the metric below, Q times for each symbol estimate:

$$\left|\hat{S}_k - S_q\right|_{q=1,\ldots,Q} \tag{38}$$

Accordingly, this decoder is linear on the received signals and its complexity order is $O(QK)$. This is in contrast with a complexity order of $O(Q^K)$ for the nonlinear strict maximum likelihood decoder which is based on the computation of the metric D_K given below, for all K-tuples of possible vectors in the constellation.

$$D_K = \sum_{k=1}^{2K} \left|Y[t+k-1] - \mathbf{diag}[\boldsymbol{G}_N \cdot \boldsymbol{H}]_k\right|^2 \tag{39}$$

Note, that unlike the scenario considered here, in block-fading channels the rows of $\boldsymbol{H}$ are constant. It was shown in [12] that in this case the estimates $\hat{S}_k$ obtained with (37) are orthogonal. In other words, this linear decoder is also a maximum likelihood decoder in block-fading channels.

Unfortunately, just as with the Alamouti scheme, the orthogonality of the symbol estimates S_k are quickly lost in the presence of a non-quasi-static fading channel, such as those seen by the symbols transmitted through each carrier of an OFDM system.

Let us illustrate this with an example. Consider Tarokh's STBC for four antennas ($\boldsymbol{G}_4$). In a non-quasi-static fading channel, $\boldsymbol{R}$ becomes

$$\boldsymbol{R} = \begin{bmatrix} \boldsymbol{R}_{1,1} & 0 \\ 0 & \boldsymbol{R}_{2,2} \end{bmatrix} \tag{40}$$

where

$$\boldsymbol{R}_{1,1} = \begin{bmatrix} H_1[t] & H_2[t] & H_3[t] & H_4[t] \\ H_2[t+1] & -H_1[t+1] & H_4[t+1] & -H_3[t+1] \\ H_3[t+2] & -H_4[t+2] & -H_1[t+2] & H_2[t+2] \\ H_4[t+3] & H_3[t+3] & -H_2[t+3] & -H_1[t+3] \end{bmatrix} \tag{41}$$

$$\boldsymbol{R}_{2,2} = \begin{bmatrix} H_1[t+4] & H_2[t+4] & H_3[t+4] & H_4[t+4] \\ H_2[t+5] & -H_1[t+5] & H_4[t+5] & -H_3[t+5] \\ H_3[t+6] & -H_4[t+6] & -H_1[t+6] & H_2[t+6] \\ H_4[t+7] & H_3[t+7] & -H_2[t+7] & -H_1[t+7] \end{bmatrix} \tag{42}$$

The linear combination of received signals yielding the estimate for, say, the first symbol S_1 is:

$$\begin{aligned} \hat{S}_1 = & H_1[t]^* \cdot Y[t] + H_2[t+1]^* \cdot Y[t+1] \\ & + H_3[t+2]^* \cdot Y[t+2] + H_4[t+3]^* \cdot Y[t+3] \\ & + H_1[t+4] \cdot Y[t+4]^* + H_2[t+5] \cdot Y[t+5]^* \\ & + H_3[t+6] \cdot Y[t+6]^* + H_4[t+7] \cdot Y[t+7]^* \end{aligned} \tag{43}$$

Substituting (34) into (44) we have:

$$\begin{aligned}\hat{S}_1 = &\left(\sum_{k=1}^{K}|H_k[t+k-1]|^2+\sum_{k=1}^{K}|H_k[t+k+K-1]|^2\right)S_1\\ &+(H_1[t]^*H_2[t]-H_1[t+5]^*H_2[t+5]\\ &+H_1[t+4]H_2[t+4]^*-H_1[t+1]H_2[t+1]^*\\ &+H_3[t+7]^*H_4[t+7]-H_3[t+2]^*H_4[t+2]\\ &+H_3[t+3]H_4[t+3]^*-H_3[t+6]H_4[t+6]^*)S_2\\ &+(H_1[t]^*H_3[t]-H_1[t+6]^*H_3[t+6]\\ &+H_1[t+4]H_3[t+4]^*-H_1[t+2]H_3[t+2]^*\\ &+H_2[t+5]H_4[t+5]^*-H_2[t+3]H_4[t+3]^*\\ &+H_2[t+1]^*H_4[t+1]-H_2[t+7]^*H_4[t+7])S_3\\ &+(H_1[t]^*H_4[t]-H_1[t+7]^*H_4[t+7]\\ &+H_1[t+4]H_4[t+4]^*-H_1[t+3]H_4[t+3]^*\\ &+H_2[t+6]^*H_3[t+6]-H_2[t+1]^*H_3[t+1]\\ &+H_2[t+2]H_3[t+2]^*-H_2[t+5]H_3[t+5]^*)S_4\end{aligned} \tag{44}$$

Comparing equations (22) and (44) it is readily seen that this extension of the linear decoder originally proposed in [6] is really an extension of the maximum diversity combiner for the Alamouti scheme discussed in Section 3.2. As the latter, this linear decoder reduces to a linear maximum likelihood decoder in block-fading channels. However, in a non-quasi-static fading channel, the symbol estimates obtained with this method are no longer orthogonal and consequently, symbol-by-symbol maximum likelihood decoding is no longer achievable.

4.2 Partially orthogonal linear combiner

In this Section, a partially orthogonal linear decoding method for orthogonal STBCs in fast-fading channels is introduced. In order to gain insight, we start by applying Li's method to the Alamouti STBC. The decoding matrices $\boldsymbol{R}$ and $\mathcal{R}$ below relate to the pair of equations (22) and (23) and to the pair of equations (26) and (27), respectively.

$$\boldsymbol{R}=\begin{bmatrix}H_1[t] & H_2[t] & 0 & 0\\ 0 & 0 & H_2[t+1] & -H_1[t+1]\end{bmatrix} \tag{45}$$

$$\mathcal{R}=\begin{bmatrix}H_1[t+1] & H_2[t+1] & 0 & 0\\ 0 & 0 & H_2[t] & -H_1[t]\end{bmatrix} \tag{46}$$

The matrix (45), in association with equations (36) and (37) yield equations (22) and (23). Analogously, the matrix (46), together with equations (36) and (37), yield equations (26) and (27). Comparing these two matrices, it is readily seen that the entries $H_1[t]$ and $H_1[t+1]$ are permutated, with the signs + and − preserved at their original positions in both matrices. The same can be seen about the values $H_2[t]$ and $H_2[t+1]$.

Given the results shown in Section 3.3, using the matrix (46) with equations (36) and (37) yields orthogonal estimates of S_1 and S_2. This suggests that a similar strategy of permutation on the entries of (40) can be applied to derive several modified versions of $\boldsymbol{R}$, each related to the estimation of a symbol S_k, free of the interference from any other arbitrary symbol S_q, and *vice versa*.

Hereafter, we shall use the notation $\mathcal{R}_{(k,q)}$ in reference to a matrix obtained from permutations over $\boldsymbol{R}$, which yields mutually or orthogonal estimates of the pair of symbols (S_k, S_q). The set of permutations over $\boldsymbol{R}$ so as to obtain $\mathcal{R}_{(k,q)}$ is summarised as follows.

- Select the kth column of $\boldsymbol{R}_{1,1}$ and the qth column of $\boldsymbol{R}_{2,2}$;
- Denote these C_k and $C_{\tilde{q}}$, respectively;
- Permutate the values $H_n[t+i]\in C_k$ and $H_n[t+j]\in C_{\tilde{q}}$, for all n;
- Select the qth column of $\boldsymbol{R}_{1,1}$ and the kth column of $\boldsymbol{R}_{2,2}$;
- Denote these C_q and $C_{\tilde{k}}$, respectively;
- Permutate the values $H_n[t+i]\in C_q$ and $H_n[t+j]\in C_{\tilde{k}}$, for all n.

An estimate of S_k, orthogonal to S_q (denoted $\hat{S}_{k\tilde{q}}$ and read S_k *not* S_q) is then obtained by substituting $\mathcal{R}_{(k,q)}$ for $\boldsymbol{R}$ in (36), and then using (37).

Note that in STBCs from orthogonal designs, an even number K of different symbols are encoded in each block, even if an odd number of diversity branches (antennas) is used. Consequently, the matrices $\boldsymbol{R}_{1,1}$ and $\boldsymbol{R}_{2,2}$ also have even orders. From this fact, and from the fact that the above algorithm only operates on a pair of columns in $\boldsymbol{R}_{1,1}$ and $\boldsymbol{R}_{2,2}$, it is clear that a single permuted matrix $\mathcal{R}$ can be constructed to support the mutually orthogonal decoding of other pairs of symbols (S_u, S_w) such that ($u\neq k,q,w$) and ($w\neq k,q,u$). Generally, let $\mathcal{K}$ be a set of mutually exclusive pairs (i,j) such that $i\neq j$ and no other element in $\mathcal{K}$ contains i or j. Then, a single matrix $\mathcal{R}_{\mathcal{K}}$ can be constructed to yield the mutually orthogonal decoding of all pairs in $\mathcal{K}$.

As an example, let us reconsider Tarokh's $\boldsymbol{G}_4$ code. Let $\mathcal{K}=\{(1,2),(3,4)\}$ The matrix $\mathcal{R}_{\mathcal{K}}$ that yields the mutually orthogonal decoding of the pair (S_1, S_2) and of the pair (S_3, S_4) is given by

$$\boldsymbol{R}=\begin{bmatrix}\mathcal{R}_{\mathcal{K}1,1} & 0\\ 0 & \mathcal{R}_{\mathcal{K}2,2}\end{bmatrix} \tag{47}$$

where

$$\mathcal{R}_{\mathcal{K}1,1}=\begin{bmatrix}H_1[t+5] & H_2[t+5] & H_3[t+5] & H_4[t+5]\\ H_2[t+4] & -H_1[t+4] & H_4[t+4] & -H_3[t+4]\\ H_3[t+7] & -H_4[t+7] & -H_1[t+7] & H_2[t+7]\\ H_4[t+6] & H_3[t+6] & -H_2[t+6] & -H_1[t+6]\end{bmatrix} \tag{48}$$

$$\mathcal{R}_{\mathcal{K}2,2}=\begin{bmatrix}H_1[t+1] & H_2[t+1] & H_3[t+1] & H_4[t+1]\\ H_2[t] & -H_1[t] & H_4[t] & -H_3[t]\\ H_3[t+3] & -H_4[t+3] & -H_1[t+3] & H_2[t+3]\\ H_4[t+2] & H_3[t+2] & -H_2[t+2] & -H_1[t+2]\end{bmatrix} \tag{49}$$

If the matrix (47) is used to obtain an estimate of S_1 orthogonal to S_2 ($S_{1,\tilde{2}}$) we have the result given in (50). Note that the term on S_2 vanishes regardless of the channel values.

From equation (50), it is also noticeable that a reduction in the diversity gain attained is expected with this decoder.

This effect is similar to that found in Section 3.3 for the Alamouti code.

$$\begin{aligned}\hat{S}_{1,\bar{2}} =&(H_1[t+5]^*H_1[t]+H_2[t+4]^*H_2[t+1]\\&+H_3[t+7]^*H_3[t+2]+H_4[t+6]^*H_4[t+3]\\&+H_1[t+1]H_1[t+4]^*+H_2[t]H_2[t+5]^*\\&+H_3[t+3]H_3[t+6]^*+H_4[t+2]H_4[t+7]^*)S_1\\&+(H_1[t+5]^*H_2[t]-H_2[t+4]^*H_1[t+1]\\&+H_3[t+7]^*H_4[t+2]+H_4[t+6]^*H_3[t+3]\\&+H_1[t+1]H_2[t+4]^*-H_2[t]H_1[t+5]^*\\&+H_3[t+3]H_4[t+6]^*+H_4[t+2]H_3[t+7]^*)S_2\\&+(H_1[t+5]^*H_3[t]+H_2[t+4]^*H_4[t+1]\\&+H_3[t+7]^*H_1[t+2]-H_4[t+6]^*H_2[t+3]\\&+H_1[t+1]H_3[t+4]^*+H_2[t]H_4[t+5]^*\\&+H_3[t+3]H_1[t+6]^*-H_4[t+2]H_2[t+7]^*)S_3\\&+(H_1[t+5]^*H_4[t]-H_2[t+4]^*H_3[t+1]\\&+H_3[t+7]^*H_2[t+2]-H_4[t+6]^*H_1[t+3]\\&+H_1[t+1]H_4[t+4]^*-H_2[t]H_3[t+5]^*\\&+H_3[t+3]H_2[t+6]^*-H_4[t+2]H_1[t+7]^*)S_4\end{aligned} \tag{50}$$

It is clear that the same matrix (47) can be used to obtain $\hat{S}_{2,\bar{1}}$, $\hat{S}_{3,\bar{4}}$ and $\hat{S}_{4,\bar{3}}$.

Analogously, other partially orthogonal symbol estimates can be obtained by constructing a different set of mutually exclusive pairs $\mathcal{K}$ and then deriving the appropriate permuted matrix $\mathcal{R}_{\mathcal{K}}$. For instance, with $\mathcal{K}=\{(1,3),(2,4)\}$ we have:

$$\mathcal{R}_{\mathcal{K}1,1}=\begin{bmatrix}H_1[t+6] & H_2[t+6] & H_3[t+6] & H_4[t+6]\\ H_2[t+7] & -H_1[t+7] & H_4[t+7] & -H_3[t+7]\\ H_3[t+4] & -H_4[t+4] & -H_1[t+4] & H_2[t+4]\\ H_4[t+5] & H_3[t+5] & -H_2[t+5] & -H_1[t+5]\end{bmatrix} \tag{51}$$

$$\mathcal{R}_{\mathcal{K}2,2}=\begin{bmatrix}H_1[t+2] & H_2[t+2] & H_3[t+2] & H_4[t+2]\\ H_2[t+3] & -H_1[t+3] & H_4[t+3] & -H_3[t+3]\\ H_3[t] & -H_4[t] & -H_1[t] & H_2[t]\\ H_4[t+1] & H_3[t+1] & -H_2[t+1] & -H_1[t+1]\end{bmatrix} \tag{52}$$

Using (51) and (52) in (47), the estimates $\hat{S}_{1,\bar{3}}$, $\hat{S}_{3,\bar{1}}$, $\hat{S}_{2,\bar{4}}$ and $\hat{S}_{4,\bar{2}}$ are obtained.

Finally, we could make $\mathcal{K}=\{(1,4),(2,3)\}$ and construct the matrices below, which would yield the estimates $\hat{S}_{1,\bar{4}}$, $\hat{S}_{4,\bar{1}}$, $\hat{S}_{2,\bar{3}}$ and $\hat{S}_{3,\bar{2}}$.

$$\mathcal{R}_{\mathcal{K}1,1}=\begin{bmatrix}H_1[t+7] & H_2[t+7] & H_3[t+7] & H_4[t+7]\\ H_2[t+6] & -H_1[t+6] & H_4[t+6] & -H_3[t+6]\\ H_3[t+5] & -H_4[t+5] & -H_1[t+5] & H_2[t+5]\\ H_4[t+4] & H_3[t+4] & -H_2[t+4] & -H_1[t+4]\end{bmatrix} \tag{53}$$

$$\mathcal{R}_{\mathcal{K}2,2}=\begin{bmatrix}H_1[t+3] & H_2[t+3] & H_3[t+3] & H_4[t+3]\\ H_2[t+2] & -H_1[t+2] & H_4[t+2] & -H_3[t+2]\\ H_3[t+1] & -H_4[t+1] & -H_1[t+1] & H_2[t+1]\\ H_4[t] & H_3[t] & -H_2[t] & -H_1[t]\end{bmatrix} \tag{54}$$

The fact that the intrasymbol interference between any pair of arbitrary symbols can be avoided suggests that a fully orthogonal linear decoder must be possible, since the interference due to each symbol individually can be identified. This would enable symbol-by-symbol maximum likelihood decoding with a linear combiner.

In the following Sub-section it is shown that a systematic design of such combiners indeed exists.

4.3 Fully orthogonal linear combiner

It was shown in the proceeding Section that in the case of the Alamouti scheme, the conventional non-orthogonal combiner quickly looses performance in the presence of a non-quasi-static fading channel, but that a simple modification on that linear combiner can by applied yielding orthogonal estimates of the transmit symbols. This enables symbol-by-symbol maximum likelihood decoding in non-quasi-static fading channels, significantly reducing the decoding complexity of maximum likelihood decoding.

In the case of the generalised orthogonal STBCs, the complexity issue is even more severe. For instance, if 16 QAM is used with the code G_4, maximum likelihood decoding requires the computation of the metric given in (39), 65 536 times in order to decode a single block of four symbols!

While it is clear that (optimal) strict maximum likelihood decoding can be prohibitively complex in some cases, it is also clear that the partially orthogonal decoder derived above for generalised orthogonal STBCs in non-quasi-static channels cannot fully eliminate the error floors at high SNR scenarios. Although low-complexity is highly desired, a sub-optimal linear decoder is only acceptable if performance is not significantly sacrificed. This can be achieved if symbol-by-symbol maximum likelihood detection can be performed with a linear combiner.

In this Section, the partially orthogonal decoder of Section 4.2 is extended into a fully orthogonal linear combiner for symbol-by-symbol maximum likelihood decoding of STBCs in non-quasi-static fading channels. The proposed decoder is obtained by successively applying the partial interference cancellation scheme described above as follows:

Step 1. Choose an arbitrary symbol S_q and construct all matrices $\mathcal{R}_{(k,q)}$.

Step 2. Use the partially orthogonal method of Section 4.2 to obtain the estimates $\hat{S}_{k,\bar{q}}$, for all $k \neq q$.

Step 3. Construct a vector $Y_{\bar{q}}$ consisting of the estimates $\hat{S}_{k\neq q,\bar{q}}$, with 0 at the qth position, augmented by their respective complex conjugates (This emulates the receive signal vector of a 'virtual' encoded block in which the symbol S_q faces a null channel at every transmission).

Step 4. Construct a new channel matrix $H_{\bar{q}}$ whose entries are the coefficients multiplying each S_k in all elements of $Y_{\bar{q}}$ (These coefficients are simply combinations of the entries of the original channel matrix and therefore are known).

Step 5. Return to step 1 if more than two symbols are still mixed in each $\hat{S}_{k\neq q,\bar{q}}$.

Step 6. Apply the orthogonal decoder of Section 3.3 to all the pairs of mixed symbols.

Step 7. Repeat the procedure from the beginning, sequentially choosing different symbols to be cancelled so as to obtain orthogonal estimates of all other symbols.

At every iteration of the above algorithm, one symbol is eliminated and at the end of the process, two symbol estimates, fully orthogonal to all other symbols and to one another, are obtained. Repeating the process making different choices of which symbols are eliminates successively will yield orthogonal estimates for all S_k.

Before we proceed with an example, let us emphasise that although the systematic construction of orthogonal symbol estimates is described here by this iterative algorithm, the resulting combiner need not be iterative! Indeed, the algorithm provided need only be run *algebraically*, using the set of variables $\{H_n[t], H_n[t+1], \ldots, H_n[t+2K-1]\}$ for all $n = 1, \ldots, N$, a single time for each of Tarokh's full diversity STBCs, i.e. those where $K = N$ e.g. $\boldsymbol{G}_4$, $\boldsymbol{G}_8$. Once the symbolic calculations are done, we obtain, for the corresponding STBC, a set of $2K$ scalar functions $\boldsymbol{F}_k(\boldsymbol{H})$ on the channel matrix $\boldsymbol{H}$ (explicit forms are omitted here due to space limitations), which are used to directly combine the received signals onto orthogonal estimates for all S_k, as shown below.

$$\hat{S}_k = \sum_{i=1}^{K} \boldsymbol{F}_i(\boldsymbol{H}) \boldsymbol{Y}[t+i-1] + \sum_{i=K+1}^{2K} \boldsymbol{F}_i(\boldsymbol{H}) \boldsymbol{Y}[t+i-1]^* \tag{55}$$

Algebraic formulas obtained for the full diversity codes ($\boldsymbol{G}_4$, $\boldsymbol{G}_8$ etc.) work for the other codes where $K > N$ because these lower-order codes are simply truncations of the latter. For instance, $\boldsymbol{G}_3$ is a truncation of $\boldsymbol{G}_4$ and $\boldsymbol{G}_5$, $\boldsymbol{G}_6$ and $\boldsymbol{G}_7$ are truncations of $\boldsymbol{G}_8$ [2]. Consequently, $\mathcal{R}$ is always a $2K$-by-$2K$ matrix, only with a number of zero entries when codes of lower diversity order are used. For example, only one calculation is required for the code $\boldsymbol{G}_4$ (whose results are also valid for $\boldsymbol{G}_3$) and another for $\boldsymbol{G}_8$, with the results applicable to $\boldsymbol{G}_5$, $\boldsymbol{G}_6$ and $\boldsymbol{G}_7$.

As with the method in [6], as well as the partially orthogonal combiner of Section 4.2, the fully orthogonal method proposed here is linear on the received signals. Consequently, symbol-by-symbol maximum likelihood decoding of STBCs from orthogonal designs in non-block-fading channels [2] is achieved with (38).

Let us proceed with an example. We continue with $\boldsymbol{G}_4$ so that previous equations can be re-used. First, the interference due to an arbitrary symbol, e.g. S_4 (step 1), is removed from the estimates of the remaining symbols, in this case, S_1, S_2 and S_3. In order to simplify the notation, let us denote the matrix $\mathcal{R}$ built with $\mathcal{K} = \{(1,2),(3,4)\}$, $\mathcal{K} = \{(1,3),(2,4)\}$ and $\mathcal{K} = \{(1,4),(2,3)\}$ respectively by $\mathcal{R}_1$, $\mathcal{R}_2$ and $\mathcal{R}_3$. Then, we have (step 2)

$$\begin{aligned}
\hat{S}_{1,\bar{4}} &= \mathcal{R}_3^{*\langle 1\rangle} \cdot \boldsymbol{Y} + \mathcal{R}_3^{\langle 5\rangle} R_3{}^{\langle 5\rangle} \cdot \boldsymbol{Y}^* \\
\hat{S}_{2,\bar{4}} &= \mathcal{R}_2^{*\langle 2\rangle} \cdot \boldsymbol{Y} + \mathcal{R}_2^{\langle 6\rangle} \cdot \boldsymbol{Y}^* \\
\hat{S}_{3,\bar{4}} &= \mathcal{R}_1^{*\langle 3\rangle} \cdot \boldsymbol{Y} + \mathcal{R}_1^{\langle 7\rangle} \cdot \boldsymbol{Y}^*
\end{aligned} \tag{56}$$

where $^{\langle i\rangle}$ denotes the ith column.

Next, a new 'receive vector' is constructed using these estimates (step 3), giving:

$$\boldsymbol{Y}_{\bar{4}} = \left[\hat{S}_{1,\bar{4}}, \hat{S}_{2,\bar{4}}, \hat{S}_{3,\bar{4}}, 0, \hat{S}^*_{1,\bar{4}}, \hat{S}^*_{2,\bar{4}}, \hat{S}^*_{3,\bar{4}}, 0\right] \tag{57}$$

The elements of this vector can be written as

$$\begin{aligned}
\boldsymbol{Y}_{1,\bar{4}} &= \hat{S}_{1,\bar{4}} = H_1[t]_{\bar{4}} S_1 + H_2[t]_{\bar{4}} S_2 + H_3[t]_{\bar{4}} S_3 \\
\boldsymbol{Y}_{2,\bar{4}} &= \hat{S}_{2,\bar{4}} = H_2[t+1]_{\bar{4}} S_1 - H_1[t+1]_{\bar{4}} S_2 + H_4[t+1]_{\bar{4}} S_3 \\
\boldsymbol{Y}_{3,\bar{4}} &= \hat{S}_{3,\bar{4}} = H_3[t+2]_{\bar{4}} S_1 - H_4[t+2]_{\bar{4}} S_2 - H_1[t+2]_{\bar{4}} S_3 \\
\boldsymbol{Y}_{4,\bar{4}} &= 0 \\
\boldsymbol{Y}_{5,\bar{4}} &= \hat{S}^*_{1,\bar{4}} = H_1[t+4]_{\bar{4}} S_1^* + H_2[t+4]_{\bar{4}} S_2^* + H_3[t+4]_{\bar{4}} S_3^* \\
\boldsymbol{Y}_{6,\bar{4}} &= \hat{S}^*_{2,\bar{4}} = H_2[t+5]_{\bar{4}} S_1^* - H_1[t+5]_{\bar{4}} S_2^* + H_4[t+5]_{\bar{4}} S_3^* \\
\boldsymbol{Y}_{7,\bar{4}} &= \hat{S}^*_{3,\bar{4}} = H_3[t+6]_{\bar{4}} S_1^* - H_4[t+6]_{\bar{4}} S_2^* - H_1[t+6]_{\bar{4}} S_3^* \\
\boldsymbol{Y}_{4,\bar{4}} &= 0
\end{aligned} \tag{58}$$

Clearly, each of the quantities $H_n[t+k-1]_{\bar{4}}$ above is a known function of the entries $H_n[t+k-1]$ of $\boldsymbol{H}$. For instance, $H_1[t]_{\bar{4}}$ is given by:

$$\begin{aligned}
H_1[t]_{\bar{4}} = {} & H_1[t+7]^* H_1[t] + H_2[t+6]^* H_2[t+1] \\
& + H_3[t+6]^* H_3[t+2] + H_4[t+4]^* H_4[t+3] \\
& + H_1[t+3] H_1[t+4]^* + H_2[t+2] H_2[t+5]^* \\
& + H_3[t+1] H_3[t+6]^* + H_4[t] H_4[t+7]^*
\end{aligned} \tag{59}$$

Using these quantities, a new channel matrix $\boldsymbol{H}_{\bar{4}}$ and the corresponding squared matrix $\boldsymbol{R}_{\bar{4}}$ are built (step 4).

Another symbol, say S_3, is then chosen to be cancelled next and the calculations are repeated (steps 5 and 1). New sets $\mathcal{K} = \{(1,3)\}$ and $\mathcal{K} = \{(2,3)\}$ are constructed, for which new permuted matrices $\mathcal{R}_{2\bar{4}}$ and $\mathcal{R}_{3\bar{4}}$, are derived. The partially orthogonal decoder will then yield (step 2):

$$\begin{aligned}
\boldsymbol{Y}_{1,\{\bar{4},\bar{3}\}} &= \hat{S}_{1,\{\bar{4},\bar{3}\}} = \mathcal{R}_{2\bar{4}}^{*\langle 1\rangle} \cdot \boldsymbol{Y}_{\bar{4}} + \mathcal{R}_{2\bar{4}}^{\langle 5\rangle} \cdot \boldsymbol{Y}_{\bar{4}}^* \\
&= H_1[t]_{\{\bar{4},\bar{3}\}} S_1 + H_2[t]_{\{\bar{4},\bar{3}\}} S_2
\end{aligned} \tag{60}$$

$$\begin{aligned}
\boldsymbol{Y}_{2,\{\bar{4},\bar{3}\}} &= \hat{S}_{2,\{\bar{4},\bar{3}\}} = \mathcal{R}_{3\bar{4}}^{*\langle 2\rangle} \cdot \boldsymbol{Y}_{\bar{4}} + \mathcal{R}_{3\bar{4}}^{\langle 6\rangle} \cdot \boldsymbol{Y}_{\bar{4}}^* \\
&= H_2[t+1]_{\{\bar{4},\bar{3}\}} S_1^* - H_1[t+1]_{\{\bar{4},\bar{3}\}} S_2^*
\end{aligned} \tag{61}$$

Once more, the quantities $H_n[t+k-1]_{\{\bar{4},\bar{3}\}}$ are functions of $H_n[t+k-1]_{\bar{4}}$ and, by extension, of $H_n[t+k-1]$. Similarly, $\boldsymbol{Y}_{\bar{4}}$ are functions of $H_n[t+k-1]$ and $\boldsymbol{Y}$. Consequently, $\hat{S}_{1,\{\bar{4},\bar{3}\}}$ and $\hat{S}_{2,\{\bar{4},\bar{3}\}}$ can be written as combinations of the channel values $H_n[t+k-1]$ and the received signals $\boldsymbol{Y}$ such as in equation (55).

The orthogonal combiner for Alamouti's scheme presented in Section 3.3 can now be used to combine these signals onto orthogonal estimates of S_1 and S_2, giving (step 6):

$$\hat{S}_{1,\{\bar{4},\bar{3},\bar{2}\}} = H_1[t+1]^*_{\{\bar{4},\bar{3}\}} \boldsymbol{Y}_{1,\{\bar{4},\bar{3}\}} + H_2[t]_{\{\bar{4},\bar{3}\}} \boldsymbol{Y}^*_{2,\{\bar{4},\bar{3}\}} \tag{62}$$

$$\hat{S}_{2,\{\bar{4},\bar{3},\bar{2}\}} = H_2[t+1]^*_{\{\bar{4},\bar{3}\}} \boldsymbol{Y}_{1,\{\bar{4},\bar{3}\}} - H_1[t]_{\{\bar{4},\bar{3}\}} \boldsymbol{Y}^*_{2,\{\bar{4},\bar{3}\}} \tag{63}$$

Finally, it is evident that $\hat{S}_1$ and $\hat{S}_2$ can also be written as combinations of the channel values and the received signals as in (55). A similar procedure is followed to orthogonally decode S_3 and S_4 (step 7). The orthogonal estimates obtained are finally used in (38) for maximum likelihood decoding of all S_k.

We emphasise that this iterative follow-up of the method here shown is merely illustrative. As pointed out before, every $Y_{\{\tilde{q},\ldots\}}$ obtained along the process is a combination of $H_n[t+k-1]_{\{\tilde{q},\ldots\}}$ and S_k, and every $H_n[t+k-1]_{\{\tilde{q},\ldots\}}$ is a combination of the original channel values $H_n[t+k-1]$. In a usual implementation, once the channel is estimated (55) is used to obtain orthogonal estimates of S_k as linear combinations of the received signals with the functions $F_k(H)$ as coefficients.

Note that if the channel is quasi-stationary, the columns of H are identical, and so too are the matrices $\mathcal{R}_K$, since permutations over R do not change it at all. In this case, the first K functions $F_{k=1,\ldots,K}(H)$ are simply the entries of the kth column of $\mathcal{R}_{1,1}$ (multiplied by a constant) and the remaining K functions $F_{k=K+1,\ldots,2K}(H)$ are the entries of the kth column of $\mathcal{R}_{2,2}$ (multiplied by the same constant).

Given the arguments above, it is clear that the proposed linear combiner is really a generalisation of the maximum-ratio-like linear combiner, known for STBCs in block-fading channels [1, 6], to the more general case of non-*quasi*-static fading channels.

5 Simulation results

In this Section, simulation results comparing the proposed linear maximum likelihood decoder with the conventional linear decoder proposed in [6] and with the strict maximum likelihood decoder, are presented.

First, Fig. 5 compares the performances of Tarokh STBCs G_3 and G_6 implemented at the carriers of a 1024-carrier OFDM system transmitting BPSK symbols.

It is important to stress that the low-order (BPSK) modulation scheme (not so common in OFDM systems) is used here only so that the complexity of the strict maximum likelihood decoder is not too high, so as to enable the comparison with the proposed linear (symbol-by-symbol) maximum-likelihood method. In fact, with G_6 and QPSK, the strict maximum likelihood decoder would require the computation of as much as 4096 metrics per block.

The conventional decoder assumes that the channel is block-fading and uses only the channel estimates relative to the first symbol vector ($H_i[t]$). The maximum diversity decoder is that of [6] extended to the non-quasi-static fading channel as discussed in Section 4.1, and the proposed decoder is that presented in Section 4.3.

The data rate of the OFDM system is 10 Mbit/s. If the loss due to the guard interval is ignored, this gives a data rate of approximately 10 kbit/s per carrier. Given that both G_3 and G_6 are rate 1/2 codes, this results in a transmission rate of 0.5 bit/s/Hz and a symbol period of approximately 0.05 ms.

Perfectly uncorrelated channels were assumed at different transmit antennas and no OFDM co-channel interference due to carrier offset, symbol distortion, cross-talk or other effects were considered.

At each carrier, the channel has a Doppler frequency of $f_D = 50$ Hz. This Doppler spread corresponds, for instance, to that observed in the downlink of an OFDM system operating on the 5 GHz band towards a mobile with a speed of about 11 km/h [18]. From (6), these parameters result in an autocorrelation of 0.9999 over samples taken at the symbol rate, 0.9907 over samples taken every eight symbols (G_3 block size) and 0.9631 over samples taken every 16 symbols (G_6 block size).

In such moderate fading channels, the error floors resulting from using the conventional linear decoder occur at levels too low to be observed in the plot. Nevertheless, it is seen that the proposed decoder outperforms the other linear decoders and that the conventional (block-fading) combiner outperforms the maximum diversity combiner. These results are similar to those observed in Fig. 4 for Alamouti scheme.

Figure 5 also shows that the performance of the linear decoder is very close to that of a strict maximum likelihood decoder. In fact, for G_3, the curves for these two decoders fully overlap.

From all the discussions of Sections 3 and 4, it is expected that the gain provided by the proposed method in comparison to other linear methods is more noticeable the more severe the channel variation within a block. Given a fixed data-rate this can occur if, for instance, more carriers are used in the OFDM system (longer symbols), the mobile moves faster (larger Doppler frequency), a higher order modulation scheme is applied (longer symbols) or codes for a larger number of antennas are implemented (longer blocks).

This can be inferred from Fig. 4 but becomes more evident in Fig. 6. The plot compares the performances of Tarokh G_3 code in a channel with a Doppler frequency of $f_D = 75$ Hz (mobile speed of 16 km/h at 5 GHz) in systems employing BPSK, QPSK, and 8PSK modulation. The

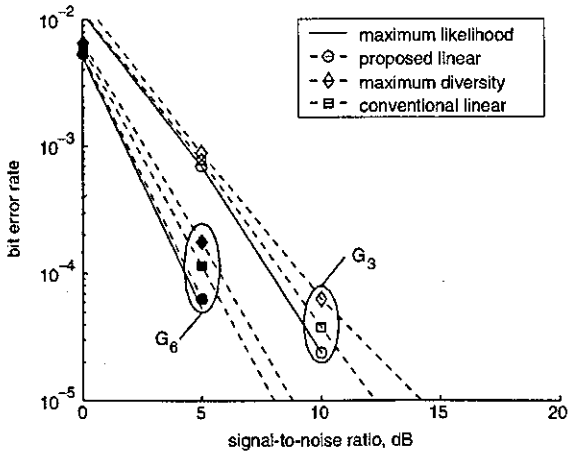

Fig. 5 *Bit error rate of Tarokh G_3 and G_6 (0.5 bit/s/Hz) STBCs with linear and maximum likelihood decoders*
Doppler frequency $f_D = 50$ Hz

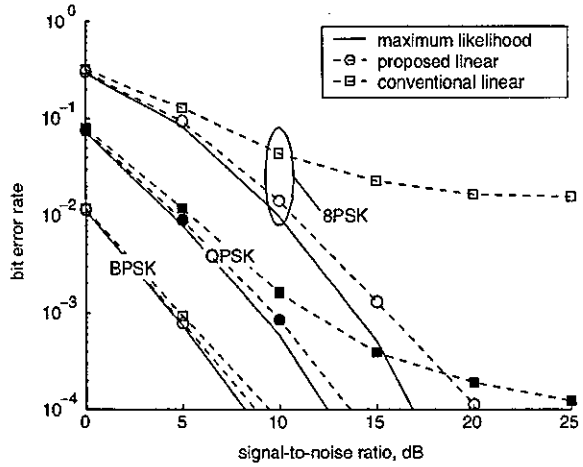

Fig. 6 *Bit error rate of Tarokh G_3 (0.5–1.5 bit/s/Hz) STBC with linear and maximum likelihood decoders*
Doppler frequency $f_D = 75$ Hz

remaining parameters (data rate, number of carriers, etc.) are all the same as described above. Curves for the maximum diversity combiner are omitted since it was already shown that this decoder actually performs worse than the conventional linear combiner at higher SNR's.

This Figure is analogous to Fig. 4 and the general results are very similar. It is confirmed that with severe channel variation within a block, in this case caused by the increase in modulation order, a higher error floor is reached by the linear decoder. As before, it is seen that the more severe the fading rate of the channel, the lower the signal-to-noise ratio where the error floor is reached. However, Fig. 4 clearly shows that the gain of the proposed combiner with respect to the conventional linear combiner is larger at more severe scenarios, since the orthogonality guaranteed by the method enables symbol-by-symbol maximum likelihood decoding. It is also evident that the price payed in terms of loss of diversity order, compared to a strict maximum likelihood decoder, is more significant in channels with faster variations within a block. Still, it is important to emphasise that the proposed decoder is expressively simpler that the strict maximum likelihood decoder. For instance, for G_3 with 8PSK, a strict maximum likelihood decoder needs to compute and compare 512 metrics per block, against only 24 required by the proposed linear method.

We emphasise that the fast fading scenario is not the target of the technique presented and is rather unlikely to be faced by high data rate OFDM systems in an urban environment. In fact, higher fading rates are associated to faster mobility, which in turn imply that the mobile must be in an area with less obstacles and at a longer distance from the base. Consequently, the typical delay spreads channels with fast mobility are likely to be small, so that the fading process in the frequency domain is less severe, which in turn imply that the STBC could rather be implemented in the alternative space-frequency arrange. This issue has been investigated in [11] and [8].

However, an important result shown in Fig. 4 is that error floors are not reached with the proposed linear decoder even at higher fading rates. This is expected since the proposed combiner ensures the orthogonality of symbol estimates at the receiver, regardless of the channel values across a block (provided that the channel is known). This can be further appreciated from the results of an illustrative simulation where the channel is considered to be constant over a symbol and vary randomly from symbol to symbol. The results are shown in Fig. 7.

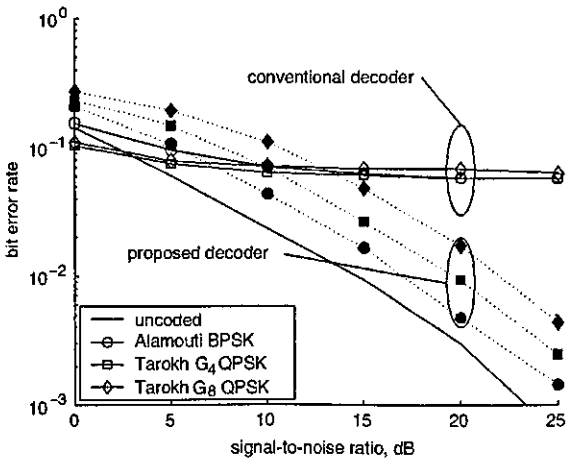

Fig. 7 *Bit error rate of Alamouti and Tarokh G_4 and G_8 STBCs with linear decoders in an illustrative fast-fading scenario*

As explained in Section 3.1, this case is purely illustrative not only because it cannot occur naturally (a truly fast-fading channel would cause severe co-channel interference in a OFDM system), but also because accurate channel estimation could not be achieved. Indeed, if the fast-fading scenario is artificially caused by interleaving, it is clear that other types of space–time codes specifically designed for such channels, e.g. [5], are be preferred. In this case, however, not only complexity is significantly increased, but realtime decoding can no longer be performed.

The illustrative simulation in a 'fast-fading' scenario has, nevertheless, the merit of demonstrating that the proposed combiner *defacto* ensures the orthogonality of symbol estimates at the receiver and translates the variation of the channel across an encoding block onto diversity loss.

The conventional decoder and the proposed maximum likelihood linear decoder were applied to Alamouti's and to Tarokh G_4 and G_8 codes in a fully random fading channel. Data-rate, number of carriers, symbol period and central carrier frequency are irrelevant information in this case, since f_D is made infinite (the channel matrix H is completely random). Results with BPSK and QPSK modulations are shown together so that all schemes run with the same transmission rate of 1 bit/s/Hz.

It is seen that while the conventional linear decoder shows a completely flat performance, the proposed linear decoder still exhibits a bit error rate performance that follows the same inclination of an uncoded (interference-free) system. While the fact that an error floor is never reached demonstrates that the proposed linear combiner yields symbol estimates which are fully orthogonal, the fact that the inclination of all curves are the same as that of an uncoded system shows that STBCs from orthogonal design with symbol-by-symbol maximum likelihood decoding do not provide any diversity gain. In other words, it can be said that the all diversity gain is traded for orthogonality in the presence of an infinitely fast-fading scenario.

In addition, the fact that the bit error rate curves translate horizontally as the order of the code (number of antennas) increases, also indicates that the proposed linear maximum likelihood decoder increases noise in the process of decoupling the symbols estimates. This noisy characteristic, which in the slower fading rates of practical interest is small enough not to be observed, is indeed typical of zero-forcing techniques such as the one presented.

6 Conclusions

A new, low-complexity linear maximum likelihood decoder for STBCs from orthogonal designs in non-quasi-static fading channels has been proposed. Non-quasi-static fading is faced by OFDM systems (which are often required to mitigate inter-symbol interference caused by frequency selectivity) in mobile channels even if these systems transmit at high-data-rates.

The proposed linear decoder is capable of obtaining orthogonal estimates for all simultaneously transmitted symbols regardless of the rate of variation of the channel within each block, provided that channel estimates are available throughout the block. It was shown that this is achieved mainly at the cost of diversity gain and some increase in noise, both relatively small for the scenarios of interest (moderate mobility).

The proposed decoder can be seen as an extension of the linear decoder proposed in [6] to the more general